

# Traces of urban forest in temperature and CO<sub>2</sub> signals in monsoon East Asia

Keunmin Lee<sup>1</sup>, Je-Woo Hong<sup>2</sup>, Jeongwon Kim<sup>1</sup>, Sungsoo Jo<sup>1</sup>, and Jinkyu Hong<sup>1</sup>

<sup>1</sup>Department of Atmospheric Sciences, Yonsei University, Seoul, 03722, Korea (Republic of)

<sup>2</sup>Korea Environment Institute, Sejong, 30147, Korea (Republic of)

*Correspondence to:* Jinkyu Hong (jhong@yonsei.ac.kr)

**Abstract.** Cities represent a key space for a sustainable society in a changing environment, and our society is steadily embracing urban green space for its role in mitigating heatwaves and anthropogenic CO<sub>2</sub> emissions. This study reports two years of surface fluxes of energy and CO<sub>2</sub> in an artificially constructed urban forest measured by the eddy covariance method to examine the impact of urban forests on air temperature and net CO<sub>2</sub> exchange. The urban forest site shows typical seasonal patterns of forest canopies with the seasonal march of the East Asian summer monsoon. This study shows that the urban forest reduces both the warming trend and urban heat island intensity compared to the adjacent high-rise urban areas and that photosynthetic carbon uptake is large despite relatively small tree density and leaf area index. During the significant drought period in the second year, gross primary production and evapotranspiration decreased, but their reduction was not as significant as those in natural forest canopies. We speculate that forest management practices, such as artificial irrigation and fertilization, enhance vegetation activity. Further analysis reveals that ecosystem respiration in urban forests is more pronounced than for typical natural forests in a similar climate zone. This can be attributed to the substantial amount of soil organic carbon due to intensive historical soil use and soil transplantation during forest construction, as well as relatively warmer temperatures in urban heat domes. Our findings suggest the need for caution in soil management when aiming to reduce CO<sub>2</sub> emissions in urban areas.

## 1 Introduction

Cities make up only 2% of the Earth's land surface but hold more than 55% of the world's population. It is expected that the urban population will reach 68% by 2050 (UN, 2019). With the unprecedented rapid urbanization in the last century, human civilization heavily depends on urban structures and functions. Current concern is regarding the disastrous impacts of climatic events (e.g., heatwaves, flooding, and drought) and environmental changes (e.g., air pollution and land degradation) on our socioeconomic system in a changing climate (McCarthy et al., 2010; Rahmstorf and Coumou, 2011). Accordingly, it remains an urgent issue to implement integrated policies for climate change mitigation and adaption toward sustainable cities against global warming and related natural disasters.

Urban green infrastructures, such as urban forests, have been recognized as a key solution toward alleviating climatic and environmental disasters (e.g., Chiesura, 2004; Haaland and van den Bosch, 2015; Oke et al., 2017;

34 Kroeger et al., 2019). Green spaces in cities are exposed to wide ranges of environmental and climatic conditions  
35 across geographical locations. Especially when green spaces replace gray infrastructures during urban  
36 redevelopment, it remains unclear whether their benefits emerge in real conditions and thereby overcome their  
37 maintenance cost and other harmful effects (e.g., allergy and ozone increase). To leverage their full potential  
38 benefits, it is necessary to assess the biophysical effects of urban forests based on direct long-term monitoring in  
39 urban areas.

40 Urban forests are a key part of green infrastructures in a city, and two of their benefits, which have been addressed  
41 in previous studies, are thermal mitigation and carbon uptake (Roy et al., 2012; Oke et al., 2017). Firstly, urban  
42 forests mitigate direct sunlight and diminish the incoming radiant energy on the land surface, thereby reducing  
43 surface temperature. Additionally, urban forests supply water to the atmosphere through transpiration and retain  
44 water for longer than the impervious surfaces of urban structures. These processes contribute to reducing air  
45 temperature by partitioning more available energy to latent heat flux ( $Q_E$ ) than sensible heat flux ( $Q_H$ ), thus  
46 creating favorable conditions for mitigating heatwaves and related health problems (e.g., Oke, 1982; Hong et al.,  
47 2019a). Eventually, this cooling effect reduces the electrical energy load by air conditioning as well as greenhouse  
48 gas emissions. Previous studies have reported cooling effects of urban forests at scales from street trees to parks  
49 (Oke et al., 1989; Bowler et al., 2010; Norton et al., 2015; Shashua-Bar and Hoffman, 2000). Such cooling effects  
50 depend not only on tree species and structures (Feyisa et al., 2014) but also on the size and vegetation density of  
51 urban green areas (Yu and Hien, 2006; Chang et al., 2007; Hamada and Ohta, 2010; Feyisa et al., 2014). However,  
52 despite the strong temperature-controlling factors of evapotranspiration (ET) and sensible heat fluxes over urban  
53 forest canopies, only a few studies have reported on surface energy balance (SEB) in urban forests in relation to  
54 thermal mitigation based on direct measurements (e.g., Oke et al., 1989; Spronken-Smith et al., 2000; Coutts et  
55 al., 2007a; Ballinas and Barradas, 2015; Hong and Hong, 2016;). Moreover, it is noticeable that forest cooling  
56 intensity depends on geography and forests can even produce a warming trend as a result of their low albedo  
57 (Bonan, 2008; Wang et al., 2018). The lack of direct urban forest measurements hinders proper assessment of  
58 their influences on the climate and environment.

59 Furthermore, urban forests mitigate anthropogenic carbon emissions by photosynthetic CO<sub>2</sub> uptake. Traditionally,  
60 carbon uptake by urban forests has been estimated by empirical relationships (e.g., biomass allometric equation)  
61 or short-term inventory of biomass data and vegetation growth rates, which have limitations of spatiotemporal  
62 coverage (Rowntree and Nowak, 1991; Nowak, 1993; Nowak et al., 2008; Weissert et al., 2014). Currently, the  
63 eddy covariance (EC) method is being applied in various ecosystems from grasslands and natural forests to urban  
64 areas because it provides continuous net CO<sub>2</sub> flux measurements at the neighborhood scale every half hour  
65 (Christen 2014). From this perspective, the EC method is useful for studying the net CO<sub>2</sub> exchange ( $F_C$ ) from  
66 diurnal to interannual variations, with its simultaneous measurement of surface energy fluxes. Recently, direct  $F_C$   
67 measurements have been performed using the EC method in urban green spaces to examine turbulent exchanges  
68 of energy and carbon (Coutts et al., 2007a, 2007b; Awal et al., 2010; Kordowski and Kuttler, 2010; Bergeron and  
69 Strachan, 2011; Crawford et al., 2011; Peters and McFadden, 2012; Velasco et al., 2013; Ward et al., 2013;  
70 Ueyama and Ando, 2016; Hong et al., 2019b). However, the EC method provides only the net effects of CO<sub>2</sub>

71 exchange from various carbon sources and sinks, which limits the physical interpretation and assessment of the  
72 benefits and costs of urban forests. It is challenging to partition  $F_C$  into individual sources and sinks in urban areas  
73 because of the complex contributions from biogenic (e.g., vegetation photosynthesis, respiration of vegetation,  
74 soil, and humans) and extra anthropogenic (e.g., fossil fuel combustion by transportation or in households and  
75 commercial buildings) processes (Pataki et al., 2003).

76 With this background, the objectives of this study include: 1) reporting temporal changes in air temperature after  
77 the artificial construction of an urban forest park in the Seoul metropolitan area with a hot and humid summer and  
78 cold and dry winter seasons and 2) quantifying the carbon uptake of urban forests based on partitioning of  $F_C$  data  
79 measured by the eddy covariance method and meteorological data (Lee et al., 2021). Here, we highlight the biotic  
80 and abiotic factors controlling the carbon cycle in urban forests and the impact of urban forests on the thermal  
81 environment after forest park construction.

## 82 **2 Materials and Methods**

### 83 **2.1 Urban surface energy and CO<sub>2</sub> balances**

84 The SEB is expressed as:

$$85 \quad Q^* + Q_F = Q_H + Q_E + \Delta Q_S + \Delta Q_A \quad (1)$$

86 where  $Q^*$  is the net all-wave radiation of the sum of outgoing and incoming short- and long-wave radiative fluxes,  
87  $Q_F$  is the anthropogenic heat flux,  $Q_H$  is the turbulent sensible heat flux,  $Q_E$  is the latent heat flux,  $\Delta Q_S$  is the net  
88 storage heat flux, and  $\Delta Q_A$  is the net heat advection (Definitions of variables in Appendix A).

89 The surface CO<sub>2</sub> budget in an urban forest is formulated as follows:

$$90 \quad F_C = E_R + E_B + RE - GPP \equiv E_R + E_B + NBE \quad (2)$$

91 where  $F_C$  is the net CO<sub>2</sub> exchange at the city-atmosphere interface,  $E_R$  and  $E_B$  are the anthropogenic CO<sub>2</sub> emissions  
92 from fossil fuel combustion by vehicles and heating in a building, respectively.  $GPP$  and  $RE$  are biotic  
93 contributions to  $F_C$ ;  $GPP$  is the gross primary production by photosynthetic CO<sub>2</sub> uptake, and  $RE$  is the ecosystem  
94 respiration. Urban ecosystem respiration considers not only the autotrophic and heterotrophic respirations of  
95 vegetation and soil but also human respiration (Moriwaki and Kanda, 2004; Velasco and Roth, 2010; Ward et al.,  
96 2013, 2015; Hong et al., 2020). Human respiration by park visitors is negligible with  $0.4 \mu\text{mol m}^{-2} \text{s}^{-1}$  at most.  
97 Additionally,  $NBE$  is the net biome CO<sub>2</sub> exchange and is typically defined as the net ecosystem exchange by  $RE$   
98  $- GPP$  for natural vegetation. Put differently,  $NBE$  refers to carbon losses in heterotrophic respiration minus the  
99 net primary production on natural vegetative surfaces; thus, negative  $NBE$  indicates the net carbon uptake by the  
100 natural ecosystem (Kirschbaum et al., 2001; Randerson et al., 2002). Unlike natural ecosystems, the  $F_C$  between  
101 an urban forest and atmosphere is a complex mixture of biogenic (i.e.,  $GPP$  and  $RE$ ) and anthropogenic (i.e.,  $E_R$   
102 and  $E_B$ ) processes across various spatial and temporal scales. In urban environments, anthropogenic emissions  
103 depend on the local characteristics (e.g., transport options, fuel types, heating demand, climate, population density,

104 levels of industrial activity, and existing carbon intensity of electricity supply) of the city (Feigenwinter et al.,  
105 2012; Kennedy et al., 2014; Lietzke et al., 2015; Stagakis et al., 2019).

106

## 107 2.2 Site description

### 108 2.2.1 Seoul Forest Park

109 Micrometeorological measurements were taken at the Seoul Forest Park (SFP) in the Seoul metropolitan area,  
110 Korea (37.5446°N, 127.0379°E). SFP is the third largest park in Seoul with an area of 1.16 km<sup>2</sup> (Fig. 1a). This  
111 area had been used as a horse racetrack and a golf course inside the track since 1950 and was surrounded by  
112 cement factories to the west (Fig. 1b). The local government initially planned this area as a commercial district  
113 with a high-rise multi-purpose building complex but changed its plan to redevelop the area as a green space in  
114 late 1990s. The construction of the SFP began in December 2003, and it was opened to the public in June 2005  
115 (Fig. 1c).

116 The mean tree height ( $h_c$ ) is approximately 7.5 m and ranges between 5.8–9.5 m. Analysis and estimation of  
117 roughness elements and integral turbulence characteristics are reported in Kent et al. (2018) and here we explain  
118 the key information on the values from Macdonald (Macdonald et al., 1998) and Kanda (Kanda et al., 2013)  
119 methods with vegetation in Kent et al., 2017. 1-m horizontal resolution digital terrain and digital surface model  
120 data are analyzed for roughness parameters and tree heights. The mean roughness length ( $z_0$ ) and zero-plane  
121 displacement height ( $z_d$ ) range between 0.3–0.6 and 4.1–8.2 m with wind directions, respectively.  $z_0$  and  $z_d$  have  
122 seasonal and directional variations depending on the variability of the leaves on the vegetation (Lee, 2015; Kent  
123 et al., 2018).  $z_0$  and  $z_d$  change from approximately 0.6 and 5.0 m during leaf-on period (June–August) to 1.2 and  
124 3.0 m during the leaf-off periods (December–February).

125 Approximately 80% of the footprint area of the SFP tower is within 250 m (Fig. 1e) and the dominant land cover  
126 within this range is a deciduous forest with irrigated grass lawns (*Zoysia*), oak (*Quercus acutissima*), ginkgo  
127 (*Ginkgo biloba*), and ash trees (*Fraxinus rhynchophylla*), which correspond to the Local Climate Zone (LCZ) ‘A’,  
128 dense trees (Stewart and Oke, 2012). The maximum leaf area index (LAI) of 300 × 300 m<sup>2</sup> around the SFP tower  
129 is approximately 1.6 (Copernicus Service information, 2020). On the east side (0–120°), there are trees  
130 (approximately 230 stems ha<sup>-1</sup>) with a small artificial lake and grasslands beyond it. Trees mainly occupy the  
131 south and west sectors of a tower (120–330°) within a 100-m radius area (approximately 540 stems ha<sup>-1</sup>) and  
132 traffic roads lie outside of the park (Fig. 1f).

133 The measurement system was installed on the rooftop of the SFP facility building (Fig. 1d). A three-dimensional  
134 sonic anemometer (CSAT3A, Campbell Scientific, USA) and enclosed infrared gas analyzer (EC155, Campbell  
135 Scientific, USA) were mounted 12.2 m above the ground level (2.8 m above the roof of an 8.4 m high building)  
136 in June 2013 for 2 years (Fig. 1d). The eddy covariance data were recorded using the data logger (CR3000,  
137 Campbell Scientific, USA) with a 10-Hz sampling rate and a 30-min averaging time. The gas analyzer was  
138 calibrated with standard CO<sub>2</sub> gas every three months. The measurement height ( $z_m$ ) satisfied the tower height

139 requirement over forested or more structurally complex ecosystems in most of wind directions (i.e.,  $z_m \cong z_d + 4(h_c$   
140  $- z_d)$ ) and turbulent flow is in the skimming flow region (Grimmond and Oke, 1999; Munger et al., 2012; Kent et  
141 al., 2018). Turbulent flow can be in the wake regime in the west direction (210–330°) during non-growing season  
142 (Grimmond and Oke, 1999). Two radiometers (NR Lite2 and CMP3, Kipp & Zonen, Netherlands) were used to  
143 measure the radiative fluxes. An auxiliary measurement included a humidity and temperature probe (HMP155A,  
144 Vaisala, Finland) and EVI (Enhanced Vegetation Index) by in situ LED sensors.

145 The roads consist of eight and ten lanes carrying heavy traffic throughout the day (~100,000 vehicles day<sup>-1</sup>) to the  
146 south and west of the tower (Fig. 1c). Hourly traffic volume, which is used for surface flux partitioning, is  
147 evaluated on the road adjacent to the SFP tower every year by the Seoul Metropolitan Government  
148 (<https://topis.seoul.go.kr>). Across the road on the western side of the tower, a cement factory still exists, although  
149 its size is smaller than it used to be in the past (Fig. 1b and 1c).

150

### 151 **2.2.2 Climate conditions**

152 Climatic condition shows a distinct seasonal variation with the seasonal march of the East Asian summer monsoon  
153 (Fig. 2). The mean climatological values (1981-2010) of the screen-level air temperature ( $T_{air}$ ) and precipitation  
154 were 12.5°C and 1450 mm year<sup>-1</sup>, respectively. During the study period (June 2013–May 2015), the observed  $T_{air}$   
155 was higher than the climatological mean. Higher temperatures lasted longer in the summer of 2013 with the  
156 stagnation of the migratory anticyclones (June) and North Pacific anticyclone (July–August). There were strong  
157 heatwaves in the spring seasons of 2014 and 2015 (Hong et al., 2019a). Wind direction also shows seasonal  
158 variation with the monsoon system. Prevailing wind is southwesterly in spring and summer and changes to  
159 northeasterly in autumn and northwesterly in winter (Fig. 3). Main wind comes from vegetative surface in the  
160 park, but other land cover types are included differently with seasons. Accordingly, road fraction in flux footprint  
161 is larger in spring and summer and building emission is included only winter season with northeasterly wind (Fig.  
162 1f and 2).

163 Notably, seasonal precipitation shows a contrasting pattern between two consecutive years (Fig. 2d). In the first  
164 year (June 2013–May 2014), annual precipitation was 1256 mm, which corresponded to approximately 90% of  
165 the climatological mean. In addition, approximately 50% of the annual rainfall was concentrated in the summer  
166 with an estimated 650 mm occurring only in July 2013; however, in the second year the annual rainfall was 932  
167 mm (i.e., 67% of the climatological mean) (i.e., the smallest annual precipitation in the past 20 years). The monthly  
168 precipitation values in the July and August of 2014 were 198 and 169 mm, respectively, which represented only  
169 approximately 35% of the climate mean. Accordingly, the vapor pressure deficit ( $VPD$ ) and downward shortwave  
170 radiation ( $K_d$ ) in July 2013 were relatively smaller than those in July 2014 (Fig. 2b and 3c).

171

### 172 2.2.3 Observations in the Seoul Metropolitan Area

173 Meteorological data from six stations (one eddy covariance station, one aerodrome meteorological observation  
174 station, and four automatic weather stations) in the Seoul Metropolitan Area are analyzed to examine the heat  
175 mitigation and CO<sub>2</sub> reduction effects of urban vegetation in the SFP (Table 1 and Fig. 1a). The Eunpyeong eddy  
176 covariance site (EP, 37.6350°N, 126.9287°E) is for surface flux observations in the northwest of Seoul, where  
177 there was a recent urban redevelopment to high-rise and high-population residential areas from low-rise areas  
178 (Hong and Hong, 2016; Hong et al., 2019b). Flux observations at the site have been conducted since 2012, and  
179 they show the surface energy fluxes and turbulence characteristics of a typical urban residential area. Because the  
180 area around the SFP was originally planned to be redeveloped to high-rise high-population residential buildings,  
181 EP is selected for comparative analysis as an antipodal place for the SFP region because the sites are close to each  
182 other and so have the similar synoptic conditions.

183 The Gimpo Airport weather station (GP, 37.5722°N, 126.7751°E) is located on the western boundary of Seoul,  
184 and it is surrounded by grasslands and croplands, which corresponds to LCZ 'D'. As the dominant wind comes  
185 from the west, the GP site is generally affected by the same synoptic weather conditions as Seoul. The GP station  
186 represents the rural environment of the Seoul Metropolitan Area because urban development is restricted around  
187 the airport. In this study, we select the GP site as a reference point and calculate the urban heat island intensity  
188 (UHI<sub>i</sub>) as the synchronous difference in  $T_{air}$  between the urban and rural areas accordingly (Stewart, 2011).

189 The Seongdong weather station (SD, 37.5472°N, 127.0389°E), the closest station to the SFP, is located  
190 approximately 300 m north of the SFP tower (Fig. 1c). Since the station began observations in August 2000, the  
191 meteorological data at SD are useful for analyzing temperature changes before and after the construction of the  
192 SFP. Accordingly, it is used to analyze local climatic changes caused by the SFP. Moreover, SD provides auxiliary  
193 weather variables (e.g., precipitation) that are not observed in SFP station and reference data for the gap filling.

194 The Gangnam, Seocho, and Songpa weather stations (hereafter denoted as CBD) are located in Seoul's central  
195 business district, which corresponds to LCZ 1 or 2. These sites are also close to the SFP (~ 5 km); thus,  
196 temperatures in these regions can be assumed to be exposed to the same synoptic condition. The annual mean  
197 maximum UHI<sub>i</sub> of CBD ranges from 3.7 to 5 °C and is similar to that of the SD. These regions show greater UHI<sub>i</sub>  
198 than other parts of Seoul because of dense skyscrapers (Hong et al., 2013; Hong et al., 2019a). The average  
199 temperature of these three automatic weather stations is used to evaluate the temperature and UHI<sub>i</sub> reduction  
200 effects of the SFP construction. All meteorological data from the automatic weather station and aerodrome  
201 meteorological observation station are observed every minute, and they are averaged for 1 h for UHI<sub>i</sub> analysis.  
202 All the meteorological data are processed for quality control on the National Climate Data Portal of the Korea  
203 Meteorological Administration (<http://data.kma.go.kr>).

### 204 2.3 Data processing procedures

205 Turbulent fluxes are computed using EddyPro (6.2.0 version, LI-COR), with the applications of the double  
206 rotation, time lag compensation using covariance maximization, quality test, and spectral corrections (Hong et al.,

207 2020 and references therein). We apply the following post processes for quality control: 1) plausible value check,  
208 2) spike removal, and 3) discarding the negative  $F_C$  flux during the nighttime (i.e., no photosynthesis at night)  
209 (Hong et al., 2020). Negative nocturnal  $F_C$  occurs occasionally ( $n = 485$ ) and its accumulated value is 1.4 % of  
210 the total  $F_C$ . The total study period from installation (31 May, 2013) to termination (03 June, 2015) is  
211 approximately 2 years (35,174 potential 30-min data), and in December 2013, there was a gap for approximately  
212 4 weeks due to the power system failure. The total available data are approximately 90.1%, 88.3%, and 85.4% ( $n$   
213 = 31,709, 31,064, and 30,028) for  $Q_H$ ,  $Q_E$ , and  $F_C$ , respectively.

214 The flux partitioning and gap filling methods are well documented in previous studies of Lee et al. (2021) and  
215 Hong et al. (2019b) and here we describe the core of the methods. Missing values in turbulent exchange of energy  
216 and  $\text{CO}_2$  are filled with an artificial neural network (ANN) of a backpropagation algorithm. The ANN uses the  
217 cosine transformed time-of-the-day and day-of-the-year, air temperature, relative humidity, wind speed and  
218 direction, atmospheric pressure, precipitation, downward shortwave radiation, cloud cover, soil temperature, and  
219 EVI.

220 Flux partitioning into photosynthesis and ecosystem respiration from the EC measured  $F_C$  requires additional  
221 information and data processing (e.g., Stoy et al., 2006). Stochastic  $F_C$  partitioning methods were recently applied  
222 by reprocessing EC observation data with auxiliary data and provided useful knowledge on carbon cycle (Hiller  
223 et al., 2011; Crawford and Christen, 2015; Menzer and McFadden, 2017; Stagakis et al., 2019). Here we partition  
224 the measured  $F_C$  into four contributing components (i.e.,  $RE$ ,  $GPP$ ,  $E_R$ , and  $E_B$  in Eq. 2) to investigate their biotic  
225 and abiotic controlling factors in an artificially constructed park. Menzer and McFadden (2017) estimates  
226 anthropogenic emissions with traffic volume and air temperature in winter with wind directions when  
227 anthropogenic emission is dominant in net  $\text{CO}_2$  fluxes. This study extends the statistical partitioning method by  
228 Menzer and McFadden (2017). Similar to Menzer and McFadden (2017), our partitioning method chooses  
229 temporal subsets so that some components in Eqn. (2) are insignificant with footprint weighted road fraction so  
230 that the statistical partitioning is applicable even when  $E_R$  is not negligible. In this way,  $RE$  is estimated as a  
231 function of temperature first and GPP is finally estimated after modelling  $E_R$  and  $E_B$  based on the traffic volume  
232 and high-resolution footprint weighted road fraction (see Fig. 3a and Table 1 in Lee et al. (2021)). Our estimations  
233 on anthropogenic emission from vehicle and building show good correlation with inventory data such as visitor  
234 counts, traffic volume, and natural gas consumption in the park. More information and relevant figures on the flux  
235 partitioning are available in Lee et al. (2021).

## 236 **3 Results and discussion**

### 237 **3.1 Surface energy fluxes**

238 Surface energy fluxes at the SFP shows typical seasonal variations over natural forest canopies with the seasonal  
239 march of the East Asian monsoon (Fig. 4) (Hong and Kim, 2011; Hong et al., 2019b; Hong et al., 2020). There  
240 are lengthy rainy spells and large temporal variabilities of meteorological conditions during the East Asian  
241 summer monsoon period (Fig. 3d). This heavy rainfall causes substantial decreases in  $K_L$ , and thus  $Q^*$ , with large

242 temporal variations, thereby leading to the mid-summer depression of surface fluxes (Fig. 3c and 4).  $Q^*$  also  
243 reaches its maximum in spring rather than in summer and decreases gradually from spring to winter (Fig. 4). The  
244 annual ration of  $Q_E$  to  $Q^*$  at the SFP is smaller than its global average of 0.55 and values over forest canopies at  
245 similar latitudes in the East Asia (Falge et al., 2001; Suyker and Verma, 2008; Khatun et al., 2011). In summer,  
246 about 50% of  $Q^*$  is partitioned to  $Q_E$ , and  $Q_H$  is minimum because of the ample water supply from the summer  
247 rainfall.  $Q_H$  is maximum in spring and even larger in winter, despite the relatively smaller  $Q^*$ , because of the cold  
248 and dry climatic conditions induced by the winter monsoon. Accordingly, the seasonal mean Bowen ratio ( $\beta =$   
249  $\sum Q_H / \sum Q_E$ ) ranges from near zero (summer) to approximately 4 (winter) with its daily maximum around 9 in early  
250 January 2015 (Fig. 5).  $\beta$  in the SFP is consistently lower than the high-rise, high-density residential area (i.e., the  
251 EP site) because of the ET from the vegetative canopies and the unpaved surfaces in the urban forest. Daytime  
252 Bowen ratio in summer is about 0.6, which is smaller in other urban sites but is similar to suburban sites of the  
253 similar vegetation cover mainly because of the small fraction of impervious spaces around the SFP station (Table  
254 2).

255 Surface energy fluxes also shows annual variabilities influenced by the timing of the onset and duration of the  
256 summer monsoon, similarly to natural forest in East Asia, (Hong and Kim, 2011) (Fig. 3, 4, and 5). As discussed  
257 in Section 2.2.2, annual precipitation is much larger in the first year than in the second year because of the  
258 interannual variations in the East Asian summer monsoon activity, thereby making substantial differences in  
259 surface radiative fluxes. Furthermore,  $Q_E$  shows the difference between the first and second years of the  
260 observation, particularly by responding to such interannual variability of radiation. In the first year,  $Q_E$  is more  
261 than  $300 \text{ W m}^{-2}$  and has a relatively larger temporal variability because of the frequent rainfall events in summer,  
262 compared to the second year. However, it is notable that interannual variability of surface fluxes are relatively  
263 weaker than natural forest in this region which will be better manifested in ET and its ratio to precipitation.

264 Evapotranspiration rate, which is equivalent to  $Q_E$ , ranges from  $5 \text{ mm month}^{-1}$  in January 2015 to  $74 \text{ mm month}^{-1}$   
265 in August 2013, and the annual ET values are  $367$  and  $320 \text{ mm year}^{-1}$  in the first and second years, respectively  
266 (Fig. 3 and 5 and Table 3). The ET values correspond to 29.3% and 34.3% of the annual precipitations and 49 %  
267 and 42% of net radiation, respectively. The annual ET in the second year is smaller than that in the first year with  
268 extensive drought in the second year. The difference in ET between the two consecutive years (i.e., 48 mm) mainly  
269 occurred in summer (42 mm), especially in August (30 mm) (Fig. 5). However, the ET in the second year shows  
270 only an approximately 12% decrease, despite a substantial decrease in precipitation (26% decrease) and the similar  
271 net radiation in the second year, compared to the first year (Table 3). Although the summer monsoon provides  
272 ample water to the ecosystem, its delay and weakness result in severe drought and stress to the ecosystem in this  
273 region (Hong and Kim, 2011); however, such ecosystem stress, such as the shrinking of ET and carbon uptake,  
274 has not been extensively investigated for the urban forest. We speculate that artificial irrigation by a sprinkler  
275 mitigated ecosystem stress to a certain degree in the urban forest.



### 276 3.2 Urban heat island intensity

277 The influence of urban forests on summer temperature is evident in UHI. Apparently, the UHI of the SFP (UHI<sup>S</sup>  
278 hereafter) and CBD (UHI<sup>C</sup> hereafter) gradually increases after mid-afternoon and is the largest at night (Fig. 6).  
279 This diurnal pattern is consistent with previous reports in cities exposed to different geographical and climatic  
280 conditions because rural areas cool faster than urban areas (Oke et al., 2017). Additionally, UHI<sup>C</sup> is positive  
281 throughout all days ranging from 0.2–2.2 °C (i.e., warmer than rural area, GP) and is greater than UHI<sup>S</sup> by 0–  
282 1.5 °C. The reason for this stronger UHI<sup>C</sup> is that the CBD stations are in the central business district; thus, the  
283 densities of buildings surrounding these stations are much higher than those surrounding the SFP station. At night  
284 (19:00–06:00), UHI<sup>C</sup> and UHI<sup>S</sup> are approximately 1.8 °C and 1.4 °C, respectively. The maximum UHI difference  
285 between the CBD and SFP was 0.7 °C in 2013 and 0.5 °C in 2014.

286 Around sunrise, sharp declines in the UHI are observed because the air temperature near the urban area increases  
287 relatively slowly as urban fabrics, such as asphalt, brick, and concrete, have larger heat capacities and lower sky  
288 view factors than the rural areas (Oke et al., 2017). Eventually, this slow increase in the air temperature reduces  
289 the differences in  $T_{air}$  among the stations, thereby reducing the UHI. The minimum UHI<sup>C</sup> values were 0.3 °C  
290 (2013) at 09:30 and 0.2 °C (2014) at 08:30, while the minimum UHI<sup>S</sup> occurs at 10:30 with values of –0.1 °C  
291 (2013) and 0.0 °C (2014). This implies that the timing of the minimum UHI is delayed in the SFP compared to  
292 the CBD. Notably, when there is strong ET (i.e., the first year) and more time is required to warm the SFP surface,  
293 the urban-rural difference in thermal admittance becomes relatively small. This can be attributed to the higher  
294 thermal capacity of the wetter soil of the SFP because of artificial irrigation and the absence of impervious surfaces  
295 (Oke et al., 1991). The diurnal variations in UHI<sup>S</sup> also show the interannual variability in both amplitude and  
296 steepness over the two consecutive years. Despite the similar summertime UHI<sup>C</sup> for both years, the daytime  
297 UHI<sup>S</sup> in 2013 was approximately 0.2 °C lower than that in 2014. Notably, the summer  $Q_E$  was greater in 2013  
298 than in 2014, and this observed summertime asymmetric difference between the SFP and CBD stations was not  
299 found in the winter when ET was negligible (not shown here).

300  $\Delta T_{air}$  is always positive during the entire summer season (i.e., CBD is warmer than SD) and shows distinct impacts  
301 on magnitude and diurnal variability after the park construction (Fig. 7). This difference will be larger if we  
302 consider that the measurement height at the CBD is higher than that at the SD (Table. 1). Notably, this temperature  
303 contrast mainly occurs in the afternoon when ET is dominant. The maximum  $\Delta T_{air}$  is approximately 0.3 °C around  
304 10:00 before the park construction (Fig. 7a) and increases up to approximately 0.5 °C with its peak occurrence  
305 shifting from the morning to the afternoon (i.e., around 14:00) after the construction (Fig. 7b). This peak time in  
306 the afternoon is coincident with the time when photosynthesis and  $Q_E$  are highest. The annual mean of the  
307 maximum UHI in the SD is about 4 °C and does not change significantly after the park construction compared to  
308 the CBD regions (Hong et al., 2019a). On the contrary, the daytime maximum UHI of the SD in summer decreases  
309 after the park construction (not shown here). Our results indicate that the thermal mitigation of the urban forest is  
310 important because of the wetter soil surface of the park and subsequent increases in  $Q_E$ , compared to the  
311 impervious surfaces in urban areas. This is especially true if we consider that the SFP area was originally planned  
312 to be developed as a high-population multi-purpose building complex. Our findings emphasize that the heat

313 mitigation of the urban forest depends on the ratio of  $Q_E$  to net radiation. Indeed, there is an evident negative  
314 relationship between daytime  $Q_E$  and air temperature differences between the SFP and CBD stations (Fig. 8). As  
315  $K_{\downarrow}$  is more partitioned to  $Q_E$ ,  $T_{air}$  of the SFP decreases more than that of the CBD, and the maximum temperature  
316 difference is observed in the summer season. The SFP is cooler than the CBD by up to 0.6 °C, but the SFP is  
317 warmer than the CBD during the winter-dormant season when ET is small. Our findings confirm that urban forests  
318 are responsible for substantial changes in the thermal environment in terms of  $Q_H$  and  $Q_E$ , as well as their related  
319 air and surface temperatures because of more evaporative cooling in green spaces compared to impervious  
320 surfaces such as roads and buildings in urban areas (Oke et al., 2017).

321

### 322 **3.3 Temporal dynamics of net CO<sub>2</sub> exchange**

323 Overall, the mean daytime  $F_C$  is negative (i.e., carbon uptake) in the summer (June–August), indicating that  
324 photosynthesis, the only carbon sink, is dominant in the growing season (Fig. 9). This carbon uptake period is  
325 coincident with the active vegetation manifested by increases in EVI (not shown here). Summertime  
326 photosynthetic carbon uptake ( $GPP$ ) has a daily average of 7.6  $\mu\text{mol m}^{-2} \text{s}^{-1}$  with a maximum of 18.9  $\mu\text{mol m}^{-2} \text{s}^{-1}$   
327 around 12:30 (Fig. 9 and 10). A daily minimum  $F_C$  also occurs around 12:30 with the maximum photosynthetic  
328 carbon uptake during this time. CO<sub>2</sub> uptake is highest in June, with a maximum of approximately 13  $\mu\text{mol m}^{-2} \text{s}^{-1}$   
329 (Fig. 9a). In the middle of summer (4th and 31st two-week data in Fig. 9a), CO<sub>2</sub> uptake decreases significantly  
330 because photosynthesis is limited because of the reduced  $K_{\downarrow}$  by cloud and rainfall with the onset of the summer  
331 monsoon (Fig. 2c). This mid-summer depression of carbon uptake has been reported in the Asian natural  
332 vegetations (e.g., Kwon et al., 2009; Hong and Kim, 2011; Hong et al., 2014). Greater reduction in CO<sub>2</sub> uptake  
333 observed in 2013 than in 2014 was attributed to a longer monsoon period in 2013. Indeed, from 8 to 21 July 2013  
334 (4th two-week data in Fig. 9a), the accumulated precipitation was approximately 400 mm for two weeks, and the  
335 daily averaged  $K_{\downarrow}$  was only 70  $\text{W m}^{-2}$ .

336 The vegetation around the SFP absorbs more CO<sub>2</sub> than is emitted by local carbon sources and  $F_C$  is negative only  
337 during the summer daytime. Because of substantial amounts of anthropogenic emissions and ecosystem  
338 respiration,  $F_C$  changes from negative (i.e., carbon sink) to positive values (i.e., carbon source) even around 16:30  
339 in summer unlike in natural ecosystems, despite the substantial downward shortwave radiation (e.g., Desai et al.,  
340 2008; Hong et al., 2009; Alekseychik et al., 2017; Chatterjee et al., 2020). As photosynthesis decreases,  $F_C$   
341 changes to positive values from November. During the non-growing season (i.e., late autumn, winter, and early  
342 spring), anthropogenic emissions were also dominant because photosynthesis and ecosystem respiration decrease  
343 with smaller  $K_{\downarrow}$  and lower temperatures. During these periods,  $F_C$  had minimum values at 04:00–05:00 and  
344 increases until 15:00–16:00. The diurnal variations in  $F_C$  mainly followed the traffic volume. There also is a clear  
345 positive relationship between  $F_C$  and  $\lambda$  (Fig. 4 in Lee et al., 2021). It is also noteworthy that the peak time of  $F_C$   
346 (16:00) is earlier than the peak time of  $\lambda$  (18:00) from December to early March because  $E_B$  is the largest at around  
347 15:00–16:00, indicating that  $E_R$  and  $E_B$  are the controlling factor of  $F_C$  in this period.

348 The seasonal  $F_C$  variation also depends on the spatio-temporal distribution of CO<sub>2</sub> sources and flux footprint  
349 because the latter covers various land use with changes in wind direction and atmospheric stability (Fig. 10). In  
350 autumn, the main wind direction changes to the north as the synoptic conditions change as discussed in section 2  
351 (Fig. 3); therefore,  $\lambda$  is smaller in autumn compared to other seasons (Fig. 9b). For example, the road fraction is  
352 smallest at < 1% from midnight to midday and < 3% during the afternoon in October and November (11th, 12th,  
353 36th, and 37th two-week data in Fig. 9b). In these periods, the nighttime  $F_C$  shows the lowest value of  
354 approximately  $2.9 \mu\text{mol m}^{-2} \text{s}^{-1}$ , which is attributable to the smallest road fraction, lower respiration, and minimal  
355 heating usage.

356 In early spring,  $\lambda$  is generally larger; thus,  $E_R$  plays a significant role in  $F_C$ , and  $E_B$  remains non-zero until early  
357 April because of anthropogenic emission by hot water and space heating in the building within the footprint,  
358 thereby resulting in the largest  $F_C$  in this period. With a shutdown of the heating system (i.e., zero  $E_B$ ) and the  
359 sprouting of leaves in April, there is a sharp decrease in  $F_C$  (Fig. 10b). From December to March, CO<sub>2</sub> emissions  
360 increase up to  $30 \mu\text{mol m}^{-2} \text{s}^{-1}$  with larger variability because of intermittent anthropogenic emissions from the  
361 park facility building in the south-west directions (due to space heating and boiling water), as well as the relatively  
362 increased contribution of vehicles on the road in the western part of the site (Fig. 10b).

363 Although the positive  $F_C$  in the winter decreases in spring, its magnitude shows directional differences (Fig. 10b).  
364 On the eastern side, the mean  $F_C$  shows a negative value in May, whereas it remains positive on the western side  
365 ( $210\text{--}270^\circ$ ) until May. These findings further indicate the different contributions of various carbon sources and  
366 sinks among the different wind directions. For the wind directions from the north to the east ( $0\text{--}120^\circ$ ),  $F_C$  shows  
367 a relatively weaker carbon sink than other directions because of the relatively low tree fraction in this direction  
368 (Fig. 10). On the southern side ( $150\text{--}180^\circ$ ) having the highest tree cover fraction, a maximum carbon uptake is  
369 about  $15 \mu\text{mol m}^{-2} \text{s}^{-1}$  in June. However, despite the dense vegetation on the south and west side ( $120\text{--}330^\circ$ ), the  
370  $F_C$  magnitude was much smaller than that of other natural forests. This is related to the anthropogenic emissions  
371 from vehicles on the roads which is discussed in section 3.5.

### 372 **3.4 Light use efficiency of biogenic CO<sub>2</sub> components**

373  $F_C$  at the SFP shows a typical light response to the photosynthetically active radiation (PAR) in a way similar to  
374 natural ecosystems in spite of anthropogenic CO<sub>2</sub> sources from vehicles (Fig. 11). However, this light response in  
375 the urban forest is a distinct contrast to  $F_C$  in high-rise high-population residential areas in Seoul under the same  
376 climatic conditions that does not respond to PAR (i.e., EP station). Importantly,  $GPP$ ,  $NBE$ , and  $F_C$  show different  
377 trends with PAR depending on the direction. As stated in Section 2.2.1 and 3.3, the western side has a higher  
378 density of trees as against more grass on the eastern side, and biotic CO<sub>2</sub> uptake from the western side is  
379 substantially larger than that on the eastern side. Accordingly, the slope of the light response curve for PAR on  
380 the western side is steeper than on the eastern side.  $F_C$  at zero PAR ( $F_{C_0}$ ) is larger on the western side ( $9.7 \mu\text{mol}$   
381  $\text{m}^{-2} \text{s}^{-1}$ ) than on the eastern side ( $5.1 \mu\text{mol m}^{-2} \text{s}^{-1}$ ) because of a contribution of  $E_R$  from roads on the western side  
382 of the tower.

383 *NBE* shows a comparable light response to natural vegetation (e.g., Schmid et al., 2003). A rectangular hyperbolic  
 384 equation has been used to examine the light response of *NBE* and elucidate the directional differences in carbon  
 385 uptake:

$$386 \quad NBE = -GPP + RE = -\frac{\alpha \cdot GPP_{sat} \cdot PAR}{GPP_{sat} + \alpha \cdot PAR} + RE \quad (3)$$

387  $\alpha$  is approximately 0.0651 and 0.0558  $\mu\text{mol CO}_2$  ( $\mu\text{mol photon}$ )<sup>-1</sup> on the western and eastern sides, respectively.  
 388 Notably,  $\alpha$  on the western side is comparable to the high initial quantum yield in crops and subtropical forests in  
 389 East Asia (Hong et al., 2019b; Emmel et al., 2020). Additionally,  $GPP_{sat}$  is 30.9 and 12.7  $\mu\text{mol m}^{-2} \text{s}^{-1}$  on the  
 390 western and eastern sides, respectively. In addition, the light saturation points are at a PAR of 1500  $\mu\text{mol m}^{-2} \text{s}^{-1}$   
 391 on the eastern side, which occur at a relatively lower PAR than on the western side. Daytime respiration estimates  
 392 from equation (3) is 6.7 and 6.3  $\mu\text{mol m}^{-2} \text{s}^{-1}$  on the western and eastern sides, respectively. Because *GPP* is related  
 393 to PAR, the difference in monthly cumulative *GPP* between the two years shows a close relationship with the  
 394 difference in the monthly sunshine duration ( $r^2 = 0.75$ , not shown here), suggesting a possible impact of change  
 395 in the onset of the summer monsoon on urban forests.

396 The magnitude of *NBE* from the western side is larger than that from a suburban area with about 50% vegetative  
 397 fraction in Montreal, Canada (Fig. 7b in Bergeron and Strachan, 2011) and  $F_C$  from a highly vegetated  
 398 environment of about 67% vegetative fraction in Baltimore, USA (Crawford et al., 2011). Also, *GPP* from the  
 399 western side is comparable to the dense forest canopies in subtropical forests in Korea (Hong et al., 2019b),  
 400 deciduous forest ecosystems (Goulden et al., 1996), and a mixed hardwood forest ecosystem (Schmid et al., 2000).  
 401 However, *NBE* from the eastern side is similar to  $F_C$  from the suburban areas of about 44%, 50%, and 64%  
 402 vegetative fraction in Swindon, UK (Ward et al., 2013) and Montreal, Canada (Bergeron and Strachan, 2011), and  
 403 Ochang, Korea in the same climate zone (Hong et al., 2019b), respectively.

### 404 **3.5 Annual budget of CO<sub>2</sub> sources and sink**

405 The annual sums of the *GPP* and *RE* in the SFP are 4.6 kgCO<sub>2</sub> m<sup>-2</sup> year<sup>-1</sup> (1244 gC m<sup>-2</sup> year<sup>-1</sup>) and 5.1 kgCO<sub>2</sub> m<sup>-2</sup>  
 406 year<sup>-1</sup> (1378 gC m<sup>-2</sup> year<sup>-1</sup>), respectively (Table 4). This photosynthetic carbon uptake is smaller than its global  
 407 mean *GPP* in natural deciduous broadleaf forests with similar annual precipitation and annual mean air  
 408 temperature (total 8 years of data from 4 sites of FLUXNET2015 dataset reported in Pastorello et al., 2020) and  
 409 similar to that of deciduous broadleaf forests in East Asia (Awal et al., 2010; Kwon et al., 2010) (Table 5).  
 410 However, we note that this *GPP* is relatively larger if we consider the low vegetation fraction and leaf area index  
 411 (LAI) at our urban park. Previous studies have shown that the *GPP* of urban vegetation is scaled with vegetation  
 412 cover fraction with an increase of about 0.7 kgCO<sub>2</sub> m<sup>-2</sup> year<sup>-1</sup> per 10% increase in vegetation cover fraction (Awal  
 413 et al., 2010; Crawford and Christen, 2015; Velasco et al., 2016; Menzer and McFadden, 2017). Indeed, *GPP* at  
 414 the SFP with a 46.6% vegetation cover fraction is approximately 1.5 kgCO<sub>2</sub> m<sup>-2</sup> year<sup>-1</sup> which is larger than values  
 415 reported in other urban sites if it is scaled with the vegetation cover fraction (Fig. 12a).

416 Despite this larger GPP resulting smaller  $F_C$  eventually, there is no substantial decrease in  $F_C$  when they are scaled  
417 by vegetation fraction, suggesting large contribution of  $RE$  (Fig. 12b). There was a linear decrease in  $F_C$  of  
418 approximately  $3.0 \text{ kgCO}_2 \text{ m}^{-2} \text{ year}^{-1}$  per 10% increase in vegetation cover fraction based on the observed  $F_C$  across  
419 an urbanization gradient (Hong et al., 2019b and references therein). The annual  $F_C$  in the SFP is not so much  
420 different from other similar cities and this scaled relationship. Meanwhile,  $RE$  at our site is much larger than that  
421 in natural temperate deciduous forests in the similar climate zone (Takanashi et al., 2005; Kwon et al., 2010) and  
422 similar to that in the urban forest in East Asia (Awal et al., 2010), as well as to the global mean  $RE$  over forests  
423 with similar annual precipitation and annual mean air temperatures (Pastorello et al., 2020). Put differently, the  
424 urban forest considered in our study is an outlier compared to other natural forest canopies and urban forests  
425 because  $RE/GPP > 1$  (Table 5). Autotrophic respiration is considered to be approximately half of GPP as a rule  
426 of thumb (Piao et al., 2010), which corresponds to approximately 45% of the  $RE$  at our site, thereby indicating a  
427 large contribution of heterotrophic respiration to  $RE$ . Indeed, it was reported that soil respiration at the same site  
428 was approximately  $4 \text{ kgCO}_2 \text{ m}^{-2} \text{ year}^{-1}$  (Bae and Ryu, 2017). The reason for the large soil organic carbon was  
429 mainly because rice cultivation was carried out in this region before the 1950s, and organic carbon-rich soil was  
430 transplanted during the SFP construction, and fertilizers were applied regularly. It has also been reported that  $RE$   
431 is enhanced in urban areas because of the relatively warmer temperature in urban regions (i.e., UHI) (Awal et al.,  
432 2010). Notably,  $Q_{10}$  (the rate by which respiration is multiplied when temperature increases by  $10 \text{ }^\circ\text{C}$ ) is about 1.9  
433 at the site and matches the  $Q_{10}$  value for ecosystem respiration ( $2.2 \pm 0.7$ ) calculated for natural forests across 42  
434 FLUXNET sites (Mahecha et al., 2010). Further analysis based on the observed  $Q_{10}$  and the UHIi at the SFP  
435 indicates that UHI leads to an approximately 5% increase in  $RE$ .

436 Seasonal variations in the strength of carbon sources and sink as well as  $F_C$  are mainly regulated by the biogenic  
437 component in summer and the anthropogenic component in winter (Fig. 13). Furthermore,  $F_C$  is minimum in June,  
438 despite the similar  $GPP$  from June to August because of the relatively smaller  $RE$  during the summer season. Even  
439 in summer, photosynthetic carbon uptake is balanced with ecosystem respiration and does not offset all biotic and  
440 anthropogenic emissions, thus resulting in positive  $F_C$  values throughout the year. In winter,  $E_B$  is dominant with  
441 negligible  $GPP$  and  $RE$  due to cold temperatures, and  $E_R$  also becomes larger than  $RE$  from November.  $E_R$  shows  
442 apparent seasonal variation in wind direction and atmospheric stability. Its magnitude is about  $0.0666 \text{ } \mu\text{mol m}^{-2}$   
443  $\text{veh}^{-1} \text{ h s}^{-1}$  in neutral condition and consistent with the value in the inventory data (Lee et al., 2021). The average  
444 monthly traffic speed for the road in front of the SFP is  $50\text{--}60 \text{ km h}^{-1}$  (based on the January 2014 data from the  
445 Seoul Metropolitan Government Traffic Speed Report), and the  $\text{CO}_2$  emission rate is approximately  $0.15 \text{ kgCO}_2$   
446  $\text{km}^{-1} \text{ veh}^{-1}$  based on the emission data at this speed (Kim et al., 2011). With the width of the ten-lane road ( $25\text{--}$   
447  $30 \text{ m}$ ), the inventory-based slope (i.e.,  $\text{CO}_2$  emission rate per vehicle per area per half-hour) is approximately in  
448 the range of  $0.0631\text{--}0.0757 \text{ } \mu\text{mol m}^{-2} \text{ veh}^{-1} \text{ half-hour s}^{-1}$  ( $\cong 150 \text{ gCO}_2 \text{ km}^{-1} \text{ veh}^{-1} \times 1/30$  or  $1/25 \text{ m}^{-1} \times 1/44 \text{ mol}$   
449  $\text{gCO}_2^{-1} \times 10^{-3} \text{ km m}^{-1} \times 10^6 \text{ } \mu\text{mol mol}^{-1} \times 1/1800 \text{ half-hour s}^{-1}$ ).

450 There is an evident yearly difference in individual carbon sources and sink in two consecutive years.  $E_B$  is mainly  
451 caused by heating buildings and hot water in park facilities using natural gas. Notably,  $E_B$  is highly correlated with  
452 gas consumption in SFP during winter on monthly basis ( $R^2 = 0.94$ ; Fig. 6 in Lee et al., 2021).  $E_B$  is smaller in the

453 first year because of the relatively smaller number of park visitors and consequently smaller gas consumption,  
454 compared to the second year. Eventually, these annual differences lead to a smaller annual mean total  $F_C$  in the  
455 first year than in the second year (Table 4).  $RE$  is maximum in the August of the first year, while it is highest in  
456 July in the second year because the monthly mean air temperature is highest in August of the first and July of the  
457 second year with annual variations in air temperature with changes in the timing and duration of the East Asian  
458 summer monsoon, of which impacts have also been reported in natural vegetation in the same region (Hong and  
459 Kim, 2011; Hong et al., 2019b).  $GPP$  in summer is relatively smaller in the first year by the mid-summer  
460 depression of solar radiation because of the elongated monsoon period but annual sums of  $GPP$  are similar in two  
461 years (Table 4 and Fig. 13).  $GPP$  does not shrink in the second year of significant drought because of ample water  
462 supply by a sprinkler. Eventually,  $F_C$  in the SFP is approximately  $3.0 \text{ kgCO}_2 \text{ m}^{-2} \text{ year}^{-1}$  less than that in recently  
463 developed high-rise high-population urban areas in Seoul. Our results suggest that efficient management of urban  
464 forests, such as regular irrigation and fertilization, can be an efficient way to adapt and mitigate climate change  
465 by increasing  $\text{CO}_2$  uptake in artificial forest constructions in East Asia.

#### 466 **4 Summary and conclusions**

467 This study reported two-year surface fluxes of energy and  $\text{CO}_2$  measured by the eddy covariance method in order  
468 to examine the role of artificially generated urban forests in mitigating air temperature and anthropogenic  $\text{CO}_2$   
469 emissions. The study area is an urban park with an artificially planted forest in the Seoul Metropolitan Area  
470 redeveloped from a racetrack and factory in the mid-2000s where is influenced by a lengthy summer rainy season  
471 during the East Asian summer monsoon. To examine the mitigation of air temperature, this study compares  
472 meteorological conditions in the urban forest with the surrounding high-rise high-population urban areas. This  
473 study applies for the ANN-based gap filling (Hong et al., 2019b; Lee et al., 2021) and a statistical  $\text{CO}_2$  flux  
474 partitioning method (Lee et al., 2021) based on temporal subsets of flux data and high-resolution footprint-  
475 weighted land use data to understand the abiotic and biotic contributions to  $F_C$ .

476 Surface energy fluxes in the SFP is influenced by the summer monsoon, and more energy is distributed to  $Q_E$  than  
477  $Q_H$  in the summer in the growing season, similarly to natural forests in this climate zone. The Bowen ratio in this  
478 urban forest ranges from near 0 (summer) to about 4 (winter), which is lower throughout the year than that of  
479 high-rise and high-density residential areas in Seoul. This suggests that the vegetation and unpaved surfaces of  
480 urban forests facilitate more evaporative cooling compared to the impervious surfaces in urban areas. During the  
481 measurement period, the second year is contrasted with the first year because of the drought compared to the  
482 normal climate condition in the first year. Notably,  $ET$  decreases in the second year, but this drop is not as much  
483 as the reduced precipitation and its related changes in radiative forcing during the drought because of the artificial  
484 irrigation by a sprinkler mitigated ecosystem.

485 It is also evident that the urban forest reduced the warming trend and  $UHI_i$  around the study area. Air temperature  
486 in the SFP is lower than the surrounding area, but this coolness is reinforced after the park was created. The  
487 warming trend diminishes after the construction of the park and is smaller than that in other urban regions in the

488 Seoul Metropolitan Area. In addition, the construction of the park delays the timing of the maximum temperature  
489 difference between the urban forest and high-rise commercial from the morning to the afternoon, coinciding with  
490 the timing of the maximum  $Q_E$ . The SFP shows a typical diurnal UHI<sub>i</sub> variation pattern, which has a higher  
491 temperature at night than in rural areas. However, the UHI<sub>i</sub> in SFP is lower by 0.6 °C in summer compared to the  
492 surrounding urban area, and the time of the minimum peak time is delayed, possibly because vegetation and  
493 permeable soils in SFP have a larger thermal capacity. Notably, UHI<sub>i</sub> decreases more in the partitioning of  
494 incoming energy into latent heat fluxes and there was cooling by 0.2 °C compared to the surrounding urban area  
495 if  $Q_E/K_1$  increased by 10% in this study.

496 Net CO<sub>2</sub> exchange at the urban forest shows typical temporal variations in natural forest canopies influenced by  
497 the East Asian summer monsoon. A mid-summer depression of carbon uptake is observed with the onset of the  
498 summer monsoon, like vegetation in the East Asian monsoon region. The *GPP* is estimated by the statistical  
499 partitioning method, and the non-zero *GPP* period is coincident with the active vegetation of the significant  
500 vegetation index. Summertime photosynthetic carbon uptake has a daily average of 7.6  $\mu\text{mol m}^{-2} \text{s}^{-1}$  with a  
501 maximum of 18.9  $\mu\text{mol m}^{-2} \text{s}^{-1}$  around 12:30. However, even during the growing season, vegetative carbon uptake  
502 is insufficient to offset anthropogenic CO<sub>2</sub> emissions and ecosystem respiration on a time scale of > 1 day. Our  
503 estimations of anthropogenic CO<sub>2</sub> emissions from vehicles and buildings agree with the estimations based on  
504 inventory data such as CO<sub>2</sub> emission rate of vehicles and monthly gas consumption, and their annual budgets each  
505 have a comparable magnitude to *GPP*.

506 Annual *GPP* of the urban forest is relatively smaller than that of the forest in East Asia exposed to similar climatic  
507 conditions because of the relatively smaller vegetation cover fraction and LAI. However, it is larger than the *GPP*  
508 expected from the relationship from previous urban studies if it is normalized by the vegetation cover fraction.  
509 *RE* is, however, much larger than that in the temperate East Asian forests and is similar to the urban forest in East  
510 Asia. We speculate that soil respiration enhances such large *RE* by relatively warmer temperatures in a city and  
511 rich soil organic carbon in the SFP. The annual mean total  $F_C$  is 7.1  $\text{kgCO}_2 \text{m}^{-2} \text{year}^{-1}$ , which is smaller than the  
512 estimate from the scaling between annual total  $F_C$  and vegetation fraction (Hong et al., 2019b). Because of the  
513 spatial heterogeneity,  $F_C$  and its components showed directional changes. *NBE* from the eastern side is similar to  
514 that in suburban areas with approximately 44%, 50%, and 64% vegetative fraction in Swindon, UK (Ward et al.,  
515 2013) and Montreal, Canada (Bergeron and Strachan, 2011), and Ochang, Korea in the same climate zone (Hong  
516 et al., 2019b), respectively. However, the *NBE* and *GPP* from the western side are comparable to dense forest  
517 canopies in subtropical forests in Korea (Hong et al., 2019b), deciduous forest ecosystems (Goulden et al., 1996),  
518 and a mixed hardwood forest ecosystem (Schmid et al., 2000).

519 Our results emphasize the important role of forest management in enhancing carbon uptake and evaporative  
520 cooling despite the low vegetation fraction. Our key findings are that urban forests in East Asia are highly  
521 influenced by the East Asian monsoon like natural forests in this region, but such influence is mitigated by  
522 artificial irrigation and fertilization in urban forests. Our results emphasize the importance of forest management  
523 for efficient carbon uptake and evaporative cooling despite the low vegetation fraction. Furthermore, our

524 observation study also indicates that caution in soil management is necessary to reduce CO<sub>2</sub> emissions in urban  
525 forests, mainly resulting from large soil organic carbon and warm environment.

526

527 *Acknowledgment.* This research was supported by the Korea Meteorological Administration Research and  
528 Development Program under Grant KMI2021-01610 and National Research Foundation of Korea Grant from the  
529 Korean Government (MSIT) (NRF-2018R1A5A1024958). All data and codes are available in Lee et al. (2021)  
530 and upon request to the corresponding author (jhong@yonsei.ac.kr / <https://eapl.yonsei.ac.kr>).

531

532



Abbreviation	Definitions	Abbreviation	Definitions
CBD	the Gangnam, Seocho, and Songpa observatories at central business district	RE	ecosystem respiration
$E_B$	CO <sub>2</sub> emission from buildings	SD	the Seongdong weather station
EC	eddy covariance	SEB	surface energy balance
EP	the Eunpyeong site	SFP	the Seoul Forest Park
$E_R$	CO <sub>2</sub> emission from vehicles on roads	$T_{air}$	the screen-level air temperature
ET	evapotranspiration	$T_{air\_CBD}$	air temperature at the CBD regions
EVI	enhanced vegetation index	$T_{air\_SD}$	air temperature at the SD
$F_C$	net CO <sub>2</sub> exchange	UHI	urban heat island
$F_{C_0}$	$F_C$ at zero PAR	UHI <sub>i</sub>	urban heat island intensity
GP	the Gimpo weather station	UHI <sub>i</sub> <sup>C</sup>	UHI <sub>i</sub> at CBD
$GPP$	gross primary production	UHI <sub>i</sub> <sup>S</sup>	UHI <sub>i</sub> at SFP
$GPP_{sat}$	potential rate of ecosystem CO <sub>2</sub> uptake	VPD	vapor pressure deficit
$K_{\downarrow}$	downward shortwave radiation	$\Delta T_{air}$	$T_{air\_CBD} - T_{air\_SD}$
LCZ	local climate zone	$\Delta Q_S$	the net storage heat flux
MAP	mean annual precipitation	$\Delta Q_A$	the net heat advection
MAT	mean annual temperature	$h_c$	mean canopy height
NBE	net biome exchange of CO <sub>2</sub> ( $RE - GPP$ )	$z_0$	mean roughness length
P	precipitation	$z_d$	zero-plane displacement height
PAR	photosynthetic active radiation	$z_m$	measurement height
$Q_E$	latent heat flux	$\alpha$	quantum yield efficiency
$Q_F$	anthropogenic heat flux	$\beta$	Bowen ratio ( $= \Sigma Q_H / \Sigma Q_E$ )

$Q_H$	sensible heat flux	$\lambda$	source area weighted road ratio
$Q^*$	net radiation	$\lambda_v$	Vegetation cover fraction
$Q_{10}$	the rate by which respiration is multiplied when temperature increases by 10°C		

534

535 **References**

- 536 Alekseychik, P., Mammarella, I., Karpov, D., Dengel, S., Terentieva, I., Sabrekov, A., Glagolev, M. and Lapshina,  
537 E.: Net ecosystem exchange and energy fluxes measured with the eddy covariance technique in a western Siberian  
538 bog. *Atmospheric Chemistry and Physics*, 17, 9333-9345, 2017.
- 539 Awal M. A, Ohta T., Matsumoto K., Toba T., Daikoku K., Hattori S., and coauthors: Comparing the carbon  
540 sequestration capacity of temperate deciduous forests between urban and rural landscapes in central Japan. *Urban*  
541 *Forestry & Urban Greening*, 9(3), 261-270, 2010.
- 542 Bae, J., and Ryu, Y.: Spatial and temporal variations in soil respiration among different land cover types under  
543 wet and dry years in an urban park. *Landscape and Urban Planning*, 167, 378–385, 2017.
- 544 Ballinas, M., and Barradas, V. L.: The urban tree as a tool to mitigate the urban heat island in Mexico City: A  
545 simple phenomenological model. *Journal of environmental quality*, 45(1), 157-166, 2016.
- 546 Balogun, A. A., Adegoke, J. O., Vezhapparambu, S., Mauder, M., McFadden, J. P. and Gallo, K.: Surface energy  
547 balance measurements above an exurban residential neighbourhood of Kansas City, Missouri. *Boundary-Layer*  
548 *Meteorology*. 133, 299-321, 2009.
- 549 Bergeron, O., and Strachan, I. B.: CO<sub>2</sub> sources and sinks in urban and suburban areas of a northern mid-latitude  
550 city. *Atmospheric Environment*, 45(8), 1564-1573, 2011.
- 551 Bonan, G. B.: Forests and climate change: forcings, feedbacks, and the climate benefits of forests. *Science*, 320,  
552 1444-1449. 2008.
- 553 Bowler, D. E., Buyung-Ali, L., Knight, T. M., and Pullin, A. S.: Urban greening to cool towns and cities: A  
554 systematic review of the empirical evidence. *Landscape and Urban Planning*, 97(3), 147-155, 2010.
- 555 Chang, C. R., Li, M. H., and Chang, S. D.: A preliminary study on the local cool-island intensity of Taipei city  
556 parks. *Landscape and Urban Planning*, 80(4), 386-395, 2007.
- 557 Chatterjee, S., Swain, C.K., Nayak, A.K., Chatterjee, D., Bhattacharyya, P., Mahapatra, S.S., Debnath, M.,  
558 Tripathi, R., Guru, P.K. and Dhal, B.: Partitioning of eddy covariance-measured net ecosystem exchange of CO<sub>2</sub>  
559 in tropical lowland paddy. *Paddy and Water Environment*, 18, 623-636, 2020.
- 560 Chiesura, A.: The role of urban parks for the sustainable city. *Landscape and Urban Planning*, 68(1), 129-138,  
561 2004.
- 562 Christen, A.: Atmospheric measurement techniques to quantify greenhouse gas emissions from cities. *Urban*  
563 *Climate*, 10, 241-260, 2014.
- 564 Christen, A. and Vogt, R.: Energy and radiation balance of a central European city. *International Journal of*  
565 *Climatology*. 24, 1395-1421, 2004.
- 566 Coutts, A. M., Beringer, J., and Tapper, N. J.: Impact of increasing urban density on local climate: Spatial and  
567 temporal variations in the surface energy balance in Melbourne, Australia. *Journal of Applied Meteorology and*  
568 *Climatology*. 46(4), 477-493, 2007a.
- 569 Coutts, A. M., Beringer, J., and Tapper, N. J.: Characteristics influencing the variability of urban CO<sub>2</sub> fluxes in  
570 Melbourne, Australia. *Atmospheric Environment*, 41(1), 51-62, 2007b.
- 571 Crawford, B., Grimmond, C. S. B., and Christen, A.: Five years of carbon dioxide fluxes measurements in a highly  
572 vegetated suburban area. *Atmospheric Environment*, 45(4), 896-905, 2011.

573 Crawford, B., and Christen, A.: Spatial source attribution of measured urban eddy covariance CO<sub>2</sub> fluxes.  
574 *Theoretical and Applied Climatology*, 119(3-4), 733-755, 2015.

575 Desai, A.R., Richardson, A.D., Moffat, A.M., Kattge, J., Hollinger, D.Y., Barr, A., Falge, E., Noormets, A., Papale,  
576 D., Reichstein, M. and Stauch, V.J.: Cross-site evaluation of eddy covariance GPP and RE decomposition  
577 techniques. *Agricultural and Forest Meteorology*, 148, 821-838, 2008.

578 Emmel, C., D'Odorico, P., Revill, A., Hörtnagl, L., Ammann, C., Buchmann, N. and Eugster, W.: Canopy  
579 photosynthesis of six major arable crops is enhanced under diffuse light due to canopy architecture. *Global Change  
580 Biology*, 26(9), 2020.

581 Falge, E., Baldocchi, D., Olson, R., Anthoni, P., Aubinet, M., Bernhofer, C., Burba, G., Ceulemans, R., Clement,  
582 R., Dolman, H., Granier, A., Gross, P., Grünwald, T., Hollinger, D., Jensen, N., Katul, G., Keronen, P., Kwalski,  
583 A., Lai, C., Law, B., Meyers, T., Moncrieff, J., Moors, E., Munger, W., Pilegaard, K., Rannik, Ü., Rebmann, C.,  
584 Suyker, A., Tenhunen, J., Tu, K., Verma, S., Vesala, T., Wilson, K., and Wofsy, S.: Gap filling strategies for long  
585 term energy flux data sets. *Agricultural and Forest Meteorology*, 107, 71-77, 2001.

586 Feigenwinter, C., Vogt, R., and Christen, A.: Eddy covariance measurements over urban areas. In *Eddy  
587 Covariance* (pp. 377-397). Springer, Dordrecht, 2012.

588 Feyisa, G. L., Dons, K., and Meilby, H.: Efficiency of parks in mitigating urban heat island effect: An example  
589 from Addis Ababa. *Landscape and Urban Planning*, 123, 87-95, 2014.

590 Goldbach, A. and Kuttler, W.: Quantification of turbulent heat fluxes for adaptation strategies within urban  
591 planning. *International Journal of Climatology*, 33, 143-159, 2013.

592 Goulden, M. L., Munger, J. W., Fan, S. M., Daube, B. C., and Wofsy, S. C.: Measurements of carbon sequestration  
593 by long-term eddy covariance: Methods and a critical evaluation of accuracy. *Global Change Biology*, 2(3), 169-  
594 182, 1996.

595 Grimmond, C. S. B. and Oke, T. R.: Comparison of heat fluxes from summertime observations in the suburbs of  
596 four North American cities. *Journal of Applied Meteorology*, 34, 873-889, 1995.

597 Grimmond, C. S. B. and Oke, T. R.: Aerodynamic properties of urban areas derived from analysis of surface form.  
598 *Journal of Applied Meteorology and Climatology*, 38, 1262-1292, 1999.

599 Haaland, C., and van Den Bosch, C. K.: Challenges and strategies for urban green-space planning in cities  
600 undergoing densification: A review. *Urban forestry & Urban Greening*, 14(4), 760-771, 2015.

601 Hamada, S., and Ohta, T.: Seasonal variations in the cooling effect of urban green areas on surrounding urban  
602 areas. *Urban Forestry & Urban Greening*, 9(1), 15-24, 2010.

603 Hansen, J., Ruedy, R., Sato, M., and Lo, K.: Global surface temperature change. *Reviews of Geophysics*, 48(4),  
604 2010.

605 Hiller, R. V., McFadden, J. P., and Kljun, N.: Interpreting CO<sub>2</sub> fluxes over a suburban lawn: the influence of  
606 traffic emissions. *Boundary-Layer Meteorology*, 138(2), 215-230, 2011.

607 Hong, J., and Kim, J.: Impact of the Asian monsoon climate on ecosystem carbon and water exchanges: a wavelet  
608 analysis and its ecosystem modeling implications. *Global Change Biology*, 17(5), 1900-1916, 2011.

609 Hong, J., Kwon, H., Lim, J., Byun, Y., Lee, J., and Kim, J.: Standardization of KoFlux eddy-covariance data  
610 processing. *Korean J. Agric. For. Meteorol.*, 11, 19-26, 2009.

611 Hong, J., Takagi, K., Ohta, T., and Kodama, Y.: Wet surface resistance of forest canopy in monsoon Asia:  
612 Implications for eddy-covariance measurement of evapotranspiration. *Hydrological Processes*, 28(1), 37-42, 2014.

613 Hong, J. W., Hong, J., Lee, S. E., and Lee, J.: Spatial distribution of urban heat island based on local climate zone  
614 of automatic weather station in Seoul metropolitan area. *Atmosphere*, 23(4), 413-424, 2013.

615 Hong, J. W., and Hong, J.: Changes in the Seoul metropolitan area urban heat environment with residential  
616 redevelopment. *Journal of Applied Meteorology and Climatology*, 55(5), 1091-1106, 2016.

617 Hong, J. W., Hong, J., Kwon, E. E., and Yoon, D.: Temporal dynamics of urban heat island correlated with the  
618 socio-economic development over the past half-century in Seoul, Korea. *Environmental Pollution*, 254, 112934,  
619 2019a.

620 Hong, J.-W., Hong, J. Chun, J., Lee, Y., Chang, L., Lee, J., Yi, K., Park, Y., Byun, B., and Joo, S.: Comparative  
621 assessment of net CO<sub>2</sub> exchange across an urbanization gradient in Korea based on in situ observation, *Carbon*  
622 *Balance and Management*, <https://doi.org/10.1186/s13021-019-0128-6>, 2019b.

623 Hong, J. W., Lee, S. D., Lee, K., and Hong, J.: Seasonal variations in the surface energy and CO<sub>2</sub> flux over a high-  
624 rise, high-population, residential urban area in the East Asian monsoon region. *International Journal of*  
625 *Climatology*, <https://doi.org/10.1002/joc.6463>, 2020.

626 Hsieh, C. I., Katul, G., and Chi, T. W.: An approximate analytical model for footprint estimation of scalar fluxes  
627 in thermally stratified atmospheric flows. *Advances in Water Resources*, 23(7), 765-772, 2000.

628 Kanda, M., Inagaki, A., Miyamoto, T., Gryschka, M., and Raasch, S.: A new aerodynamic parametrization for  
629 real urban surfaces. *Boundary Layer Meteorology*, 148, 357-377, 2013.

630 Kennedy, C. A., Ibrahim, N., and Hoornweg, D.: Low-carbon infrastructure strategies for cities. *Nature Climate*  
631 *Change*, 4(5), 343, 2014.

632 Kent, C. W., Grimmond, S., and Gatey, D.: Aerodynamic roughness parameters in cities: Inclusion of vegetation.  
633 *Journal of Wind Engineering and Industrial Aerodynamics*, 169, 168-176. 2017.

634 Kent, C. W., Lee, K., Ward, H. C., Hong, J. W., Hong, J., Gatey, D., and Grimmond, S.: Aerodynamic roughness  
635 variation with vegetation: analysis in a suburban neighbourhood and a city park. *Urban Ecosystems*, 21(2), 227-  
636 243, 2018.

637 Khatun, R., Ohta, T., Kotani, A., Asanuma, J., Gamo, M., Han, S., Hirano, T., Nakai, Y., Saigusa, N., Takagi, K.  
638 and Wang, H. (2011) Spatial variations in evapotranspiration over East Asian forest sites. I. Evapotranspiration  
639 and decoupling coefficient. *Hydrological Research Letters*, 5, 83-87, 2011.

640 Kim, Y., Woo, S.K., Park, S., Kim, M. and Han, D.: A Study on Evaluation Methodology of Greenhouse Gas and  
641 Air Pollutant Emissions on Road Network - Focusing on Evaluation Methodology of CO<sub>2</sub> and NO<sub>x</sub> Emissions  
642 from Road. Korea: The Korea Transport Institute (Annual Report), 2011.

643 Kirschbaum, M.U.F., Eamus, D., Gifford, R.M., Roxburgh, S.H. and Sands, P.J.: Definitions of some ecological  
644 terms commonly used in carbon accounting. In *Net Ecosystem Exchange Workshop*, 18-20, 2001.

645 Kroeger, T., McDonald, R. I., Boucher, T., Zhang, P., and Wang, L.: Where the people are: Current trends and  
646 future potential targeted investments in urban trees for PM<sub>10</sub> and temperature mitigation in 27 US cities.  
647 *Landscape and Urban Planning*, 177, 227-240, 2018.

648 Kordowski, K., and Kuttler, W.: Carbon dioxide fluxes over an urban park area. *Atmospheric Environment*, 44(23),  
649 2722-2730, 2010.

650 Kwon, H., Park, T. Y., Hong, J., Lim, J. H., and Kim, J.: Seasonality of Net Ecosystem Carbon Exchange in Two  
651 Major Plant Functional Types in Korea. *Asia-Pacific Journal of Atmospheric Sciences*, 45(2), 149-163, 2009.

652 Lee, K. Energy, water and CO<sub>2</sub> exchanges in an artificially constructed urban forest, Master Degree Dissertation,  
653 Yonsei University, Seoul, 2015.

654 Lee, K., Hong, J. W., Kim, J., and Hong, J.: Partitioning of net CO<sub>2</sub> exchanges at the city-atmosphere interface  
655 into biotic and abiotic components. *MethodsX*, 8, 101231, 2021.

656 Lietzke, B., Vogt, R., Feigenwinter, C., and Parlow, E.: On the controlling factors for the variability of carbon  
657 dioxide flux in a heterogeneous urban environment. *International Journal of climatology*, 35(13), 3921-3941, 2015.

658 Macdonald, R. W., Griffiths, R. F., and Hall, D. J.: An improved method for the estimation of surface roughness  
659 of obstacle arrays. *Atmospheric Environment*, 32(11), 1857-1864, 1998.

660 Mahecha, M. D., Reichstein, M., Carvalhais, N., Lasslop, G., Lange, H., Seneviratne, S. I., Vargas, R., Ammann,  
661 C., Arain, M. A., Cescatti, A., Janssens, I., Migliavacca, M., Montagnani, L., and Richardson, A.: Global  
662 convergence in the temperature sensitivity of respiration at ecosystem level. *Science*, 329(5993), 838-840, 2010.

663 McCarthy, M. P., Best, M. J., and Betts, R. A.: Climate change in cities due to global warming and urban effects.  
664 *Geophysical Research Letters*, 37(9), 2010.

665 Menzer, O., and McFadden, J. P.: Statistical partitioning of a three-year time series of direct urban net CO<sub>2</sub> flux  
666 measurements into biogenic and anthropogenic components. *Atmospheric Environment*, 170, 319-333, 2017.

667 Moriwaki, R., and Kanda, M.: Seasonal and diurnal fluxes of radiation, heat, water vapor, and carbon dioxide  
668 over a suburban area. *Journal of Applied Meteorology*, 43(11), 1700-1710, 2004.

669 Munger, J. W., Loeschner, H. W., and Luo, H.: Measurement, tower, and site design considerations. In *Eddy*  
670 *Covariance* (pp. 21-58). Springer, Dordrecht, 2012.

671 Norton, B. A., Coutts, A. M., Livesley, S. J., Harris, R. J., Hunter, A. M., and Williams, N. S.: Planning for cooler  
672 cities: A framework to prioritise green infrastructure to mitigate high temperatures in urban landscapes. *Landscape*  
673 *and Urban Planning*, 134, 127-138, 2015.

674 Nowak, D. J.: Atmospheric carbon reduction by urban trees. *Journal of Environmental Management*, 37(3), 207-  
675 217, 1993.

676 Nowak, D. J., Crane, D. E., Stevens, J. C., Hoehn, R. E., Walton, J. T., and Bond, J.: A ground-based method of  
677 assessing urban forest structure and ecosystem services. *Arboriculture and Urban Forestry*. 34 (6): 347-358., 34(6),  
678 2008.

679 Oke, T. R.: The energetic basis of the urban heat island. *Quarterly Journal of the Royal Meteorological Society*,  
680 108(455), 1-24, 1982.

681 Oke, T. R.: The micrometeorology of the urban forest. *Philosophical Transactions of the Royal Society of London*.  
682 B, Biological Sciences, 324(1223), 335-349, 1989.

683 Oke, T. R., Johnson, G. T., Steyn, D. G., and Watson, I. D.: Simulation of surface urban heat islands under 'ideal'  
684 conditions at night part 2: Diagnosis of causation. *Boundary-Layer Meteorology*, 56(4), 339-358, 1991.

685 Oke, T.R., Mills, G., Christen, A., Voogt, J.A.: *Urban Climates*. Cambridge University Press, U.K., 2017.

686 Pastorello, G., Trotta, C., Canfora, E., Chu, H., Christianson, D., Cheah, Y. W., Poindexter, C., Chen,  
687 J., Elbashandy, A., Humphrey, M., Isaac, P., Polidori, D., Ribeca, A., van Ingen, C., Zhang, L., Amiro,  
688 B., Ammann, C., Arain, M.A., Ardö, J., Arkebauer, T., Arndt, S.K., Arriga, N., Aubinet, M., Aurela,  
689 M., Baldocchi, D., Barr, A., Beamesderfer, E., Marchesini, L.B., Bergeron, O., Beringer, J., Bernhofer,  
690 C., Berveiller, D., Billesbach, D., Black, T.A., Blanken, P.D., Bohrer, G., Boike, J., Bolstad, P.V., Bonal,  
691 D., Bonnefond, J.-M., Bowling, D.R., Bracho, R., Brodeur, J., Brümmer, C., Buchmann, N., Burban, B., Burns,  
692 S.P., Buysse, P., Cale, P., Cavagna, M., Cellier, P., Chen, S., Chini, I., Christensen, T.R., Cleverly, J., Collalti,  
693 A., Consalvo, C., Cook, B.D., Cook, D., Coursolle, C., Cremonese, E., Curtis, P.S., D'Andrea, E., da Rocha,  
694 H., Dai, X., Davis, K.J., De Cinti, B., de Grandcourt, A., De Ligne, A., De Oliveira, R.C., Delpierre, N., Desai,  
695 A.R., Di Bella, C.M., di Tommasi, P., Dolman, H., Domingo, F., Dong, G., Dore, S., Duce, P., Dufrêne, E., Dunn,  
696 A., Dušek, J., Eamus, D., Eichelmann, U., ElKhidir, H.A.M., Eugster, W., Ewenz, C.M., Ewers, B., Famulari,  
697 D., Fares, S., Feigenwinter, I., Feitz, A., Fensholt, R., Filippa, G., Fischer, M., Frank, J., Galvagno, M., Gharun,  
698 M., Gianelle, D., Gielen, B., Gioli, B., Gitelson, A., Goded, I., Goeckede, M., Goldstein, A.H., Gough,  
699 C.M., Goulden, M.L., Graf, A., Griebel, A., Gruening, C., Grünwald, T., Hammerle, A., Han, S., Han,  
700 X., Hansen, B.U., Hanson, C., Hatakka, J., He, Y., Hehn, M., Heinesch, B., Hinko-Najera, N., Hörtnagl,  
701 L., Hutley, L., Ibrom, A., Ikawa, H., Jackowicz-Korczynski, M., Janouš, D., Jans, W., Jassal, R., Jiang, S., Kato,  
702 T., Khomik, M., Klatt, J., Knohl, A., Knox, S., Kobayashi, H., Koerber, G., Kolle, O., Kosugi, Y., Kotani,  
703 A., Kowalski, A., Kruijt, B., Kurbatova, J., Kutsch, W.L., Kwon, H., Launiainen, S., Laurila, T., Law,  
704 B., Leuning, R., Li, Y., Liddell, M., Limousin, J.-M., Lion, M., Liska, A.J., Lohila, A., López-Ballesteros,  
705 A., López-Blanco, E., Loubet, B., Loustau, D., Lucas-Moffat, A., Lüers, J., Ma, S., Macfarlane, C., Magliulo,  
706 V., Maier, R., Mammarella, I., Manca, G., Marcolla, B., Margolis, H.A., Marras, S., Massman, W., Mastepanov,  
707 M., Matamala, R., Matthes, J.H., Mazzenga, F., McCaughey, H., McHugh, I., McMillan, A.M.S., Merbold,  
708 L., Meyer, W., Meyers, T., Miller, S.D., Minerbi, S., Moderow, U., Monson, R.K., Montagnani, L., Moore,  
709 C.E., Moors, E., Moreaux, V., Moureaux, C., Munger, J.W., Nakai, T., Neirynek, J., Nesic, Z., Nicolini,  
710 G., Noormets, A., Northwood, M., Noretto, M., Nouvellon, Y., Novick, K., Oechel, W., Olesen, J.E., Ourcival,  
711 J.-M., Papuga, S.A., Parmentier, F.-J., Paul-Limoges, E., Pavelka, M., Peichl, M., Pendall, E., Phillips,  
712 R.P., Pilegaard, K., Pirk, N., Posse, G., Powell, T., Prasse, H., Prober, S.M., Rambal, S., Rannik, Ü., Raz-Yaseef,  
713 N., Reed, D., de Dios, V.R., Restrepo-Coupe, N., Reverter, B.R., Roland, M., Sabbatini, S., Sachs, T., Saleska,  
714 S.R., Sánchez-Cañete, E.P., Sanchez-Mejia, Z.M., Schmid, H.P., Schmidt, M., Schneider, K., Schrader,  
715 F., Schroder, I., Scott, R.L., Sedlák, P., Serrano-Ortíz, P., Shao, C., Shi, P., Shironya, I., Siebicke, L., Šigut,  
716 L., Silberstein, R., Sirca, C., Spano, D., Steinbrecher, R., Stevens, R.M., Sturtevant, C., Suyker, A., Tagesson,  
717 T., Takanashi, S., Tang, Y., Tapper, N., Thom, J., Tiedemann, F., Tomassucci, M., Tuovinen, J.-P., Urbanski,  
718 S., Valentini, R., van der Molen, M., van Gorsel, E., van Huissteden, K., Varlagin, A., Verfaillie, J., Vesala,  
719 T., Vincke, C., Vitale, D., Vygodskaya, N., Walker, J.P., Walter-Shea, E., Wang, H., Weber, R., Westermann,  
720 S., Wille, C., Wofsy, S., Wohlfahrt, G., Wolf, S., Woodgate, W., Li, Y., Zampedri, R., Zhang, J., Zhou, G., Zona,  
721 D., Agarwal, D., Biraud, S., Torn, M., and Papale, D.: The FLUXNET2015 dataset and the ONEFlux processing  
722 pipeline for eddy covariance data. *Scientific Data*, 7(1), 1-27, 2020.

723 Pataki, D. E., Bowling, D. R., and Ehleringer, J. R.: Seasonal cycle of carbon dioxide and its isotopic composition  
724 in an urban atmosphere: Anthropogenic and biogenic effects. *Journal of Geophysical Research: Atmospheres*, 108,  
725 D23, <https://doi.org/10.1029/2003JD003865>, 2003.

726 Peters, E. B., and McFadden, J. P.: Continuous measurements of net CO<sub>2</sub> exchange by vegetation and soils in a  
727 suburban landscape. *Journal of Geophysical Research: Biogeosciences*, 117, G3,  
728 <https://doi.org/10.1029/2011JG001933>, 2012.

729 Piao, S., Luyssaert, S., Ciais, P., Janssens, I. A., Chen, A., Cao, C., Fang, J., Friedlingstein, P., Luo, Y., and Wang,  
730 S.: Forest annual carbon cost: A global-scale analysis of autotrophic respiration. *Ecology*, 91(3), 652-661, 2010.

731 Rahmstorf, S., and Coumou, D.: Increase of extreme events in a warming world. *Proceedings of the National  
732 Academy of Sciences*, 108(44), 17905-17909, 2011.

733 Randerson, J.T., Chapin III, F.S., Harden, J.W., Neff, J.C. and Harmon, M.E.: Net ecosystem production: a  
734 comprehensive measure of net carbon accumulation by ecosystems. *Ecological Applications*, 12(4), 937-947,  
735 2002.

736 Raupach, M. R., Antonia, R. A., and Rajagopalan, S.: Rough-wall turbulent boundary layers, *Applied Mechanics  
737 Reviews*, 44(1), 1-25, 1991.

738 Rowntree, R. A., and Nowak, D. J.: Quantifying the role of urban forests in removing atmospheric carbon dioxide.  
739 *Journal of Arboriculture*. 17 (10): 269-275., 17(10), 1991.

740 Roy, S., Byrne, J., and Pickering, C.: A systematic quantitative review of urban tree benefits, costs, and assessment  
741 methods across cities in different climatic zones. *Urban Forestry and Urban Greening*, 11(4), 351-363, 2012.

742 Schmid, H. P., Grimmond, C. S. B., Cropley, F., Offerle, B., and Su, H. B.: Measurements of CO<sub>2</sub> and energy  
743 fluxes over a mixed hardwood forest in the mid-western United States. *Agricultural and Forest Meteorology*,  
744 103(4), 357-374, 2000.

745 Schmid, H. P., Su, H. B., Vogel, C. S., and Curtis, P. S.: Ecosystem-atmosphere exchange of carbon dioxide over  
746 a mixed hardwood forest in northern lower Michigan. *Journal of Geophysical Research: Atmospheres*, 108(D14),  
747 2003.

748 Shashua-Bar, L., and Hoffman, M. E.: Vegetation as a climatic component in the design of an urban street: An  
749 empirical model for predicting the cooling effect of urban green areas with trees. *Energy and Buildings*, 31(3),  
750 221-235, 2000.

751 Shim, C., J. Hong, J. Hong, Y. Kim, M. Kang, B. Thakuri, Y. Kim, J. Chun: Evaluation of MODIS GPP over a  
752 complex ecosystem in East Asia: A case of Gwangneung flux tower in Korea, *Advances in Space Research*, 54,  
753 2296-2308, 2014.

754 Spronken-Smith, R. A., Oke, T. R., and Lowry, W. P.: Advection and the surface energy balance across an  
755 irrigated urban park. *International Journal of Climatology: A Journal of the Royal Meteorological Society*, 20(9),  
756 1033-1047. 2000.

757 Stagakis, S., Chrysoulakis, N., Spyridakis, N., Feigenwinter, C., and Vogt, R.: Eddy Covariance measurements  
758 and source partitioning of CO<sub>2</sub> emissions in an urban environment: Application for Heraklion, Greece.  
759 *Atmospheric Environment*, 201, 278-292, 2019.



760 Stewart, I. D.: A systematic review and scientific critique of methodology in modern urban heat island literature.  
761 *International Journal of Climatology*, 31(2), 200-217, 2011.

762 Stewart, I. D., and Oke, T. R.: Local climate zones for urban temperature studies. *Bulletin of the American*  
763 *Meteorological Society*, 93(12), 1879-1900, 2012.

764 Stoy, P. C., Katul, G. G., Siqueira, M. B., Juang, J. Y., Novick, K. A., Uebelherr, J. M., and Oren, R.: An evaluation  
765 of models for partitioning eddy covariance-measured net ecosystem exchange into photosynthesis and respiration.  
766 *Agricultural and Forest Meteorology*, 141(1), 2-18, 2006.

767 Suyker, A.E. and Verma, S.B.: Interannual water vapor and energy exchange in an irrigated maize-based  
768 agroecosystem. *Agricultural and Forest Meteorology*, 148, 417-427, 2008.

769 Takanashi, S., Kosugi, Y., Tanaka, Y., Yano, M., Katayama, T., Tanaka, H., and Tani, M.. CO<sub>2</sub> exchange in a  
770 temperate Japanese cypress forest compared with that in a cool-temperate deciduous broad-leaved forest.  
771 *Ecological Research*, 20(3), 313-324, 2005.

772 Ueyama, M., and Ando, T.: Diurnal, weekly, seasonal, and spatial variabilities in carbon dioxide flux in different  
773 urban landscapes in Sakai, Japan. *Atmospheric Chemistry and Physics*, 16(22), 14727-14740, 2016.

774 United Nations, Department of Economic and Social Affairs, Population Division: *World Urbanization Prospects:*  
775 *The 2018 Revision (ST/ESA/SER.A/420)*. New York: United Nations, 2019.

776 Velasco, E., and Roth, M.: Cities as net sources of CO<sub>2</sub>: Review of atmospheric CO<sub>2</sub> exchange in urban  
777 environments measured by eddy covariance technique. *Geography Compass*, 4(9), 1238-1259, 2010.

778 Velasco, E., Roth, M., Tan, S. H., Quak, M., Nabarro, S. D. A., and Norford, L.: The role of vegetation in the  
779 CO<sub>2</sub> flux from a tropical urban neighbourhood, *Atmospheric Chemistry and Physics*, 13, 10185–10202,  
780 <https://doi.org/10.5194/acp-13-10185-2013>, 2013.

781 Velasco, E., Roth, M., Norford, L., and Molina, L. T.: Does urban vegetation enhance carbon sequestration?,  
782 *Landscape and Urban Planning*, 148, 99-107, 2016.

783 Wang, L., Lee, X., Schultz, N., Chen, S., Wei, Z., Fu, C., Gao, Y., Yang, Y, and Lin, G.: Response of surface  
784 temperature to afforestation in the Kubuqi Desert, Inner Mongolia. *Journal of Geophysical Research:*  
785 *Atmospheres*, 123, 948-964, 2018.

786 Ward, H. C., Evans, J. G., and Grimmond, C. S. B.: Multi-season eddy covariance observations of energy, water  
787 and carbon fluxes over a suburban area in Swindon, UK. *Atmospheric Chemistry and Physics*, 13(9), 4645-4666,  
788 2013.

789 Ward, H. C., Kotthaus, S., Grimmond, C. S. B., Bjorkegren, A., Wilkinson, M., Morrison, W. T. J., Evans, J. G.,  
790 Morrison, J. I. L. M and Iamarino, M.: Effects of urban density on carbon dioxide exchanges: Observations of dense  
791 urban, suburban and woodland areas of southern England. *Environmental Pollution*, 198, 186-200, 2015.

792 Weissert, L. F., Salmund, J. A., and Schwendenmann, L.: A review of the current progress in quantifying the  
793 potential of urban forests to mitigate urban CO<sub>2</sub> emissions. *Urban Climate*, 8, 100-125, 2014.

794 York D., Evensen N., Martinez M., and Delgado J.: Unified equations for the slope, intercept, and standard errors  
795 of the best straight line. *American Journal of Physics*, 72(3), 367-375, 2004.

796 Yu, C., and Hien, W. N.: Thermal benefits of city parks. *Energy and Buildings*, 38(2), 105-120, 2006.

797

798 Table 1. Details of the stations used in this study.

Sites	Location	Local climate zone	Measurement height (m)
Eddy covariance station			
SFP (Seoul Forest Park)	37.5446°N, 127.0379°E	Dense tree (LCZ <sub>A</sub> )	12.2
EP (Eunpyeong)	37.6350°N, 126.9287°E	Compact highrise (LCZ <sub>1</sub> )	30
Weather station			
SD (Seongdong)	37.5472°N, 127.0389°E	Open midrise and scatted trees (LCZ <sub>5B</sub> )	25
CBD			
(Gangnam)	37.5134°N, 127.0467°E	Compact midrise and highrise (LCZ <sub>21</sub> )	20
(Seocho)	37.4889°N, 127.0156°E	Compact highrise and open midrise (LCZ <sub>15</sub> )	13
(Songpa)	37.5115°N, 127.0967°E		43
GP (Gimpo)	37.5722°N, 126.7751°E	Low plants (LCZ <sub>D</sub> )	1.5

799

800

801 Table 2. Daytime Bowen ratio ( $\beta = Q_H/Q_E$ ) in summer at the SFP and other urban sites with vegetation cover  
 802 fraction ( $\lambda_v$ ).

Site name	$\beta$	$\lambda_v$	References
SFP	0.56	0.57	this study
Basel-Sperrstrasse	2.5	0.16	Christen and Vogt (2004)
Basel-Spaleiring	2.3	0.32	Christen and Vogt (2004)
Tucson	1.8	0.42	Grimmond and Oke (1995)
Sacramento	1.4	0.42	Grimmond and Oke (1995)
Chicago	0.8	0.44	Grimmond and Oke (1995)
Los Angeles	1.4	0.41	Grimmond and Oke (1995)
Kansas City	0.48	0.58	Balogun et al. (2009)
Oberhausen-suburban	0.36	0.69	Goldbach and Kuttler (2013)

803

804

805 Table 3. Gap-filled annual budgets for surface energy fluxes and precipitation (P).

	$ET$ (mm)	$Q_H$ (MJ m <sup>-2</sup> )	$Q_E$ (MJ m <sup>-2</sup> )	$Q^*$ (MJ m <sup>-2</sup> )	P (mm)
1 <sup>st</sup> year (2013.06 – 2014.05)	367	726	896	1797	1256
2 <sup>nd</sup> year (2014.06 – 2015.05)	320	867	781	1848	932
Mean annual sum of two-year	344	797	839	1823	1094

806

807

808 Table 4. Gap-filled annual budgets for  $F_C$  (observed by EC measurement) and its components, indicating  
 809 ecosystem respiration ( $RE$ ), photosynthetic uptake by vegetation ( $GPP$ ), vehicle emissions ( $E_R$ ), and building  
 810 emissions ( $E_B$ ). All fluxes are in  $\text{kgCO}_2 \text{ m}^{-2} \text{ year}^{-1}$ .

Sites	$F_C$	$RE$	$GPP$	$E_R$	$E_B$
1 <sup>st</sup> year (2013.06 – 2014.05)	6.6	5.1 (77%)	4.7 (70%)	5.4 (81%)	1.0 (15%)
2 <sup>nd</sup> year (2014.06 – 2015.05)	7.6	5.0 (65%)	4.5 (59%)	5.4 (71%)	1.9 (25%)
Mean annual sum of two-year	7.1	5.1 (71%)	4.6 (64%)	5.4 (76%)	1.5 (20%)

811

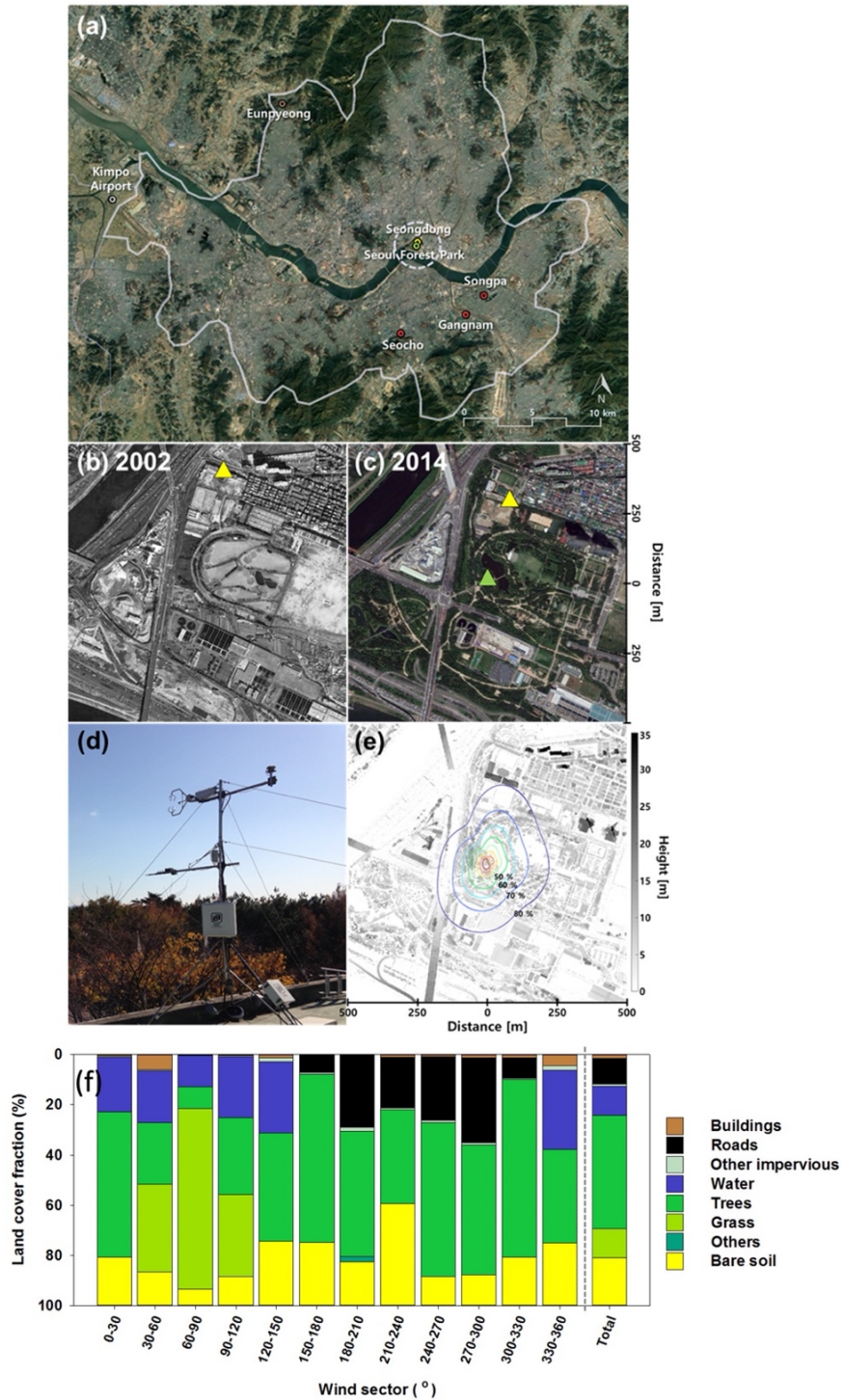
812

813 Table 5. Annual budgets of biogenic  $F_C$  components and ratios in deciduous broadleaf forests in similar climatic  
 814 conditions reported in previous studies. All fluxes are in  $\text{kgCO}_2 \text{ m}^{-2} \text{ year}^{-1}$ .

Site name	Reference	MAT (°C)	MAP (mm)	maximum LAI	<i>RE</i>	<i>GPP</i>	<i>NBE</i>	<i>RE/GPP</i>
Seoul Forest Park	This study	13.9	1094	1.6	5.1	4.6	+0.5	1.11
Nagoya urban forest	Awal et al. (2010)	15.9	1680	5.5	4.9	6.2	-1.3	0.74
Toyota rural forest		14.5	1518	4.5	2.6	4.6	-2.0	0.56
Gwangneung deciduous forest	Kwon et al. (2010)	12.8	1487	5	3.8	4.1	-0.3	0.93
Kiryu Experimental Watershed	Takanashi et al. (2005)	14.1	1309	5.5	3.9	5.6	-1.7	0.70
FLUXNET2015 dataset*	Pastorello et al. (2020)	14.5	1113		4.1	6.0	-1.9	0.68

815 \*Average value of 8-year data from 4 sites having mean annual temperature (MAT) of 12-16°C, mean annual  
 816 precipitation (MAP) of 900-2000 mm.

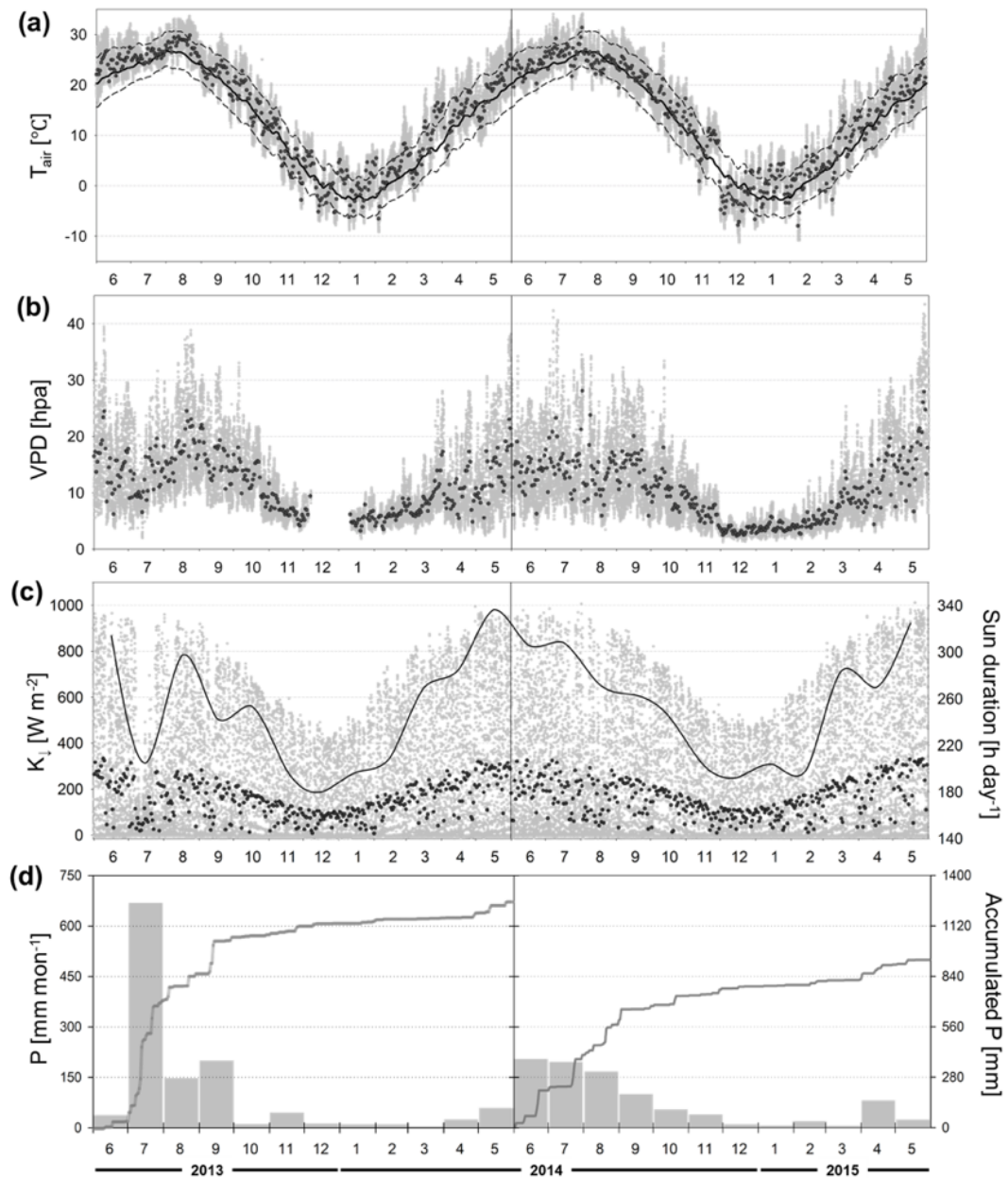
817



819

820 Figure 1. Site descriptions. (a) Location of the stations in Seoul (modified from map data © Google Earth 2019),  
 821 (b) aerial photographs around Seoul Forest Park (SFP) in 2002 before the creation of the park and (c) in 2014  
 822 during the observation period (SFP; *green triangle*, SD; *yellow triangle*), (d) photograph of the SFP station, (e)  
 823 footprint climatology (Hsieh et al., 2000) with the height of obstacles around the SFP station, and (f) land cover  
 824 fraction within a 150 m radius around the flux tower.

825

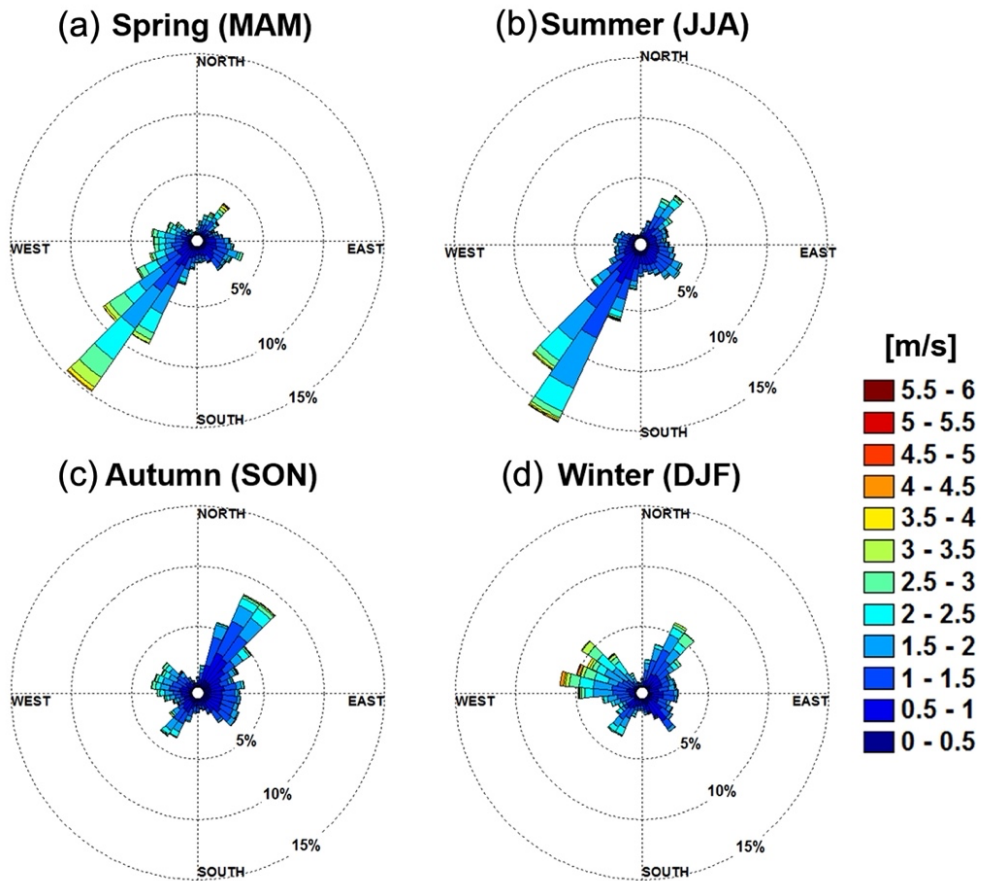


826

827 Figure 2. Climatic conditions of the SFP for two years from June 2013 to May 2015: 30-min (*gray dots*) and daily  
 828 mean (*black dots*) (a) air temperature with 30-year normal values of Seoul (daily mean; *solid line*, min and max;  
 829 *dashed lines*), (b) vapor pressure deficit (VPD) and missing data existing on December 2013, (c) downward  
 830 shortwave radiation ( $K_t$ ) and monthly averaged sunshine duration per day (*black line*), (d) monthly precipitation  
 831 (*gray bars*) and yearly accumulated precipitation (*solid line*).

832

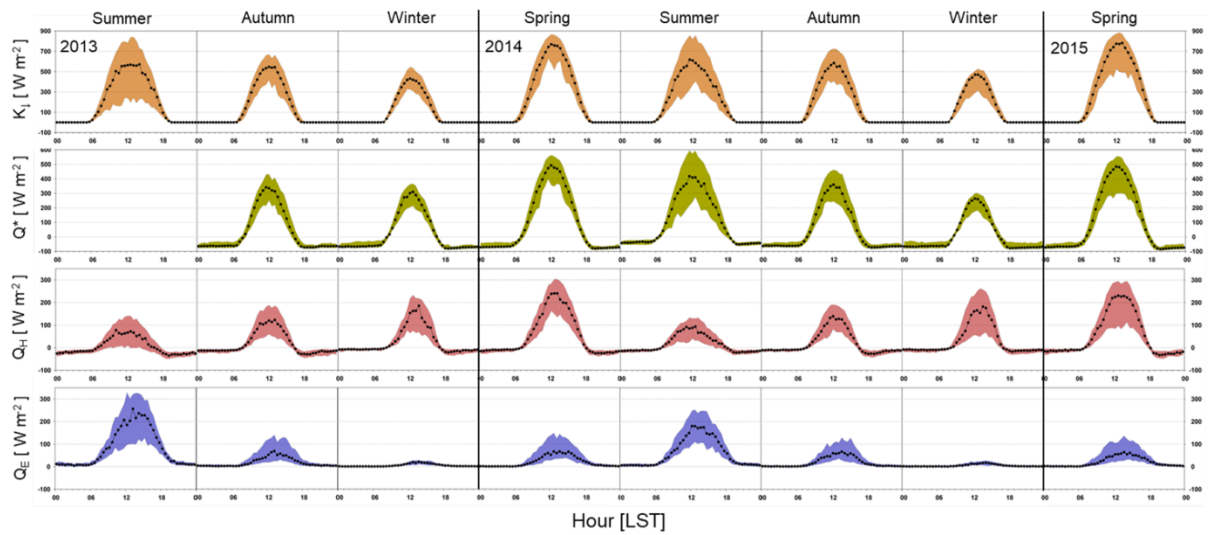




833

834 Figure 3. Wind roses with seasons: (a) spring (b) summer (c) autumn (d) winter.

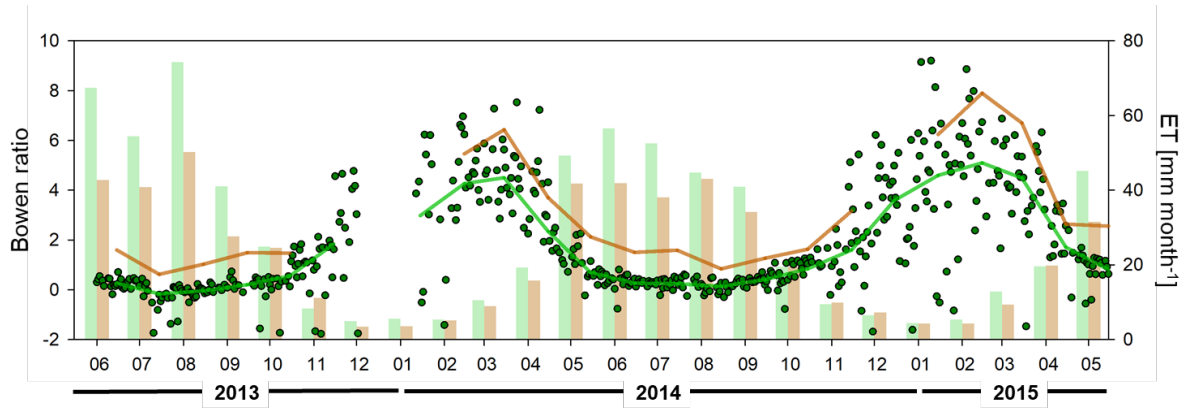
835



836

837 Figure 4. Diurnal variations of surface energy fluxes. Seasonal median diurnal variations (*points*) and interquartile  
 838 ranges (*shaded*) of 30-min downward shortwave radiation ( $K_l$ ), net radiation ( $Q^*$ ), sensible heat flux ( $Q_H$ ), and  
 839 latent heat flux ( $Q_E$ ) for two years. Since the net radiation system was installed in September 2013, there was no  
 840  $Q^*$  value in the first summer.

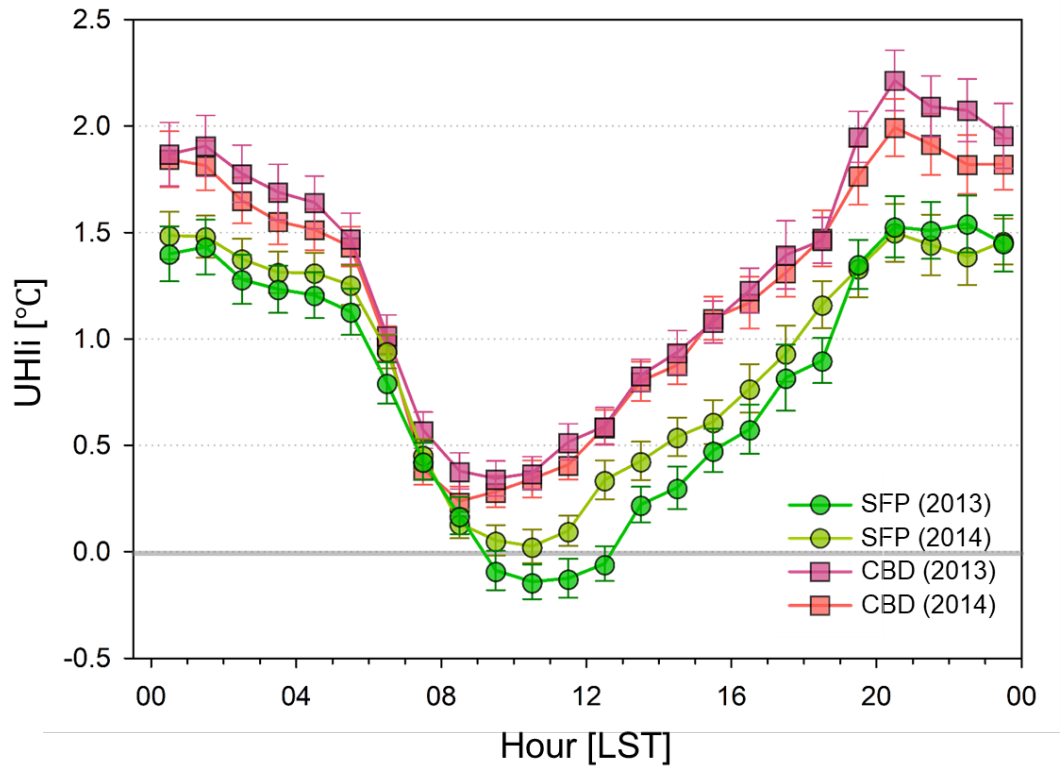
841



842

843 Figure 5. Daily Bowen ratio ( $\beta = \sum Q_H / \sum Q_E$ ; dots), monthly Bowen ratio (lines), and gap-filled monthly  
 844 evapotranspiration (ET; bars) for two years (SFP; green, EP; brown).

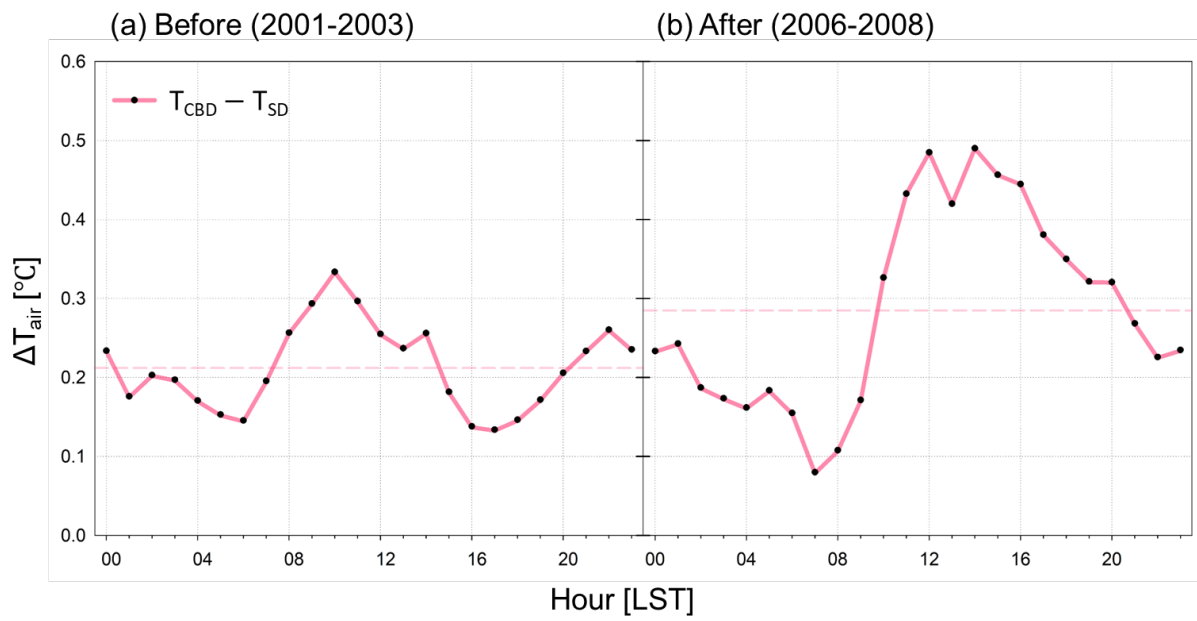
845



846

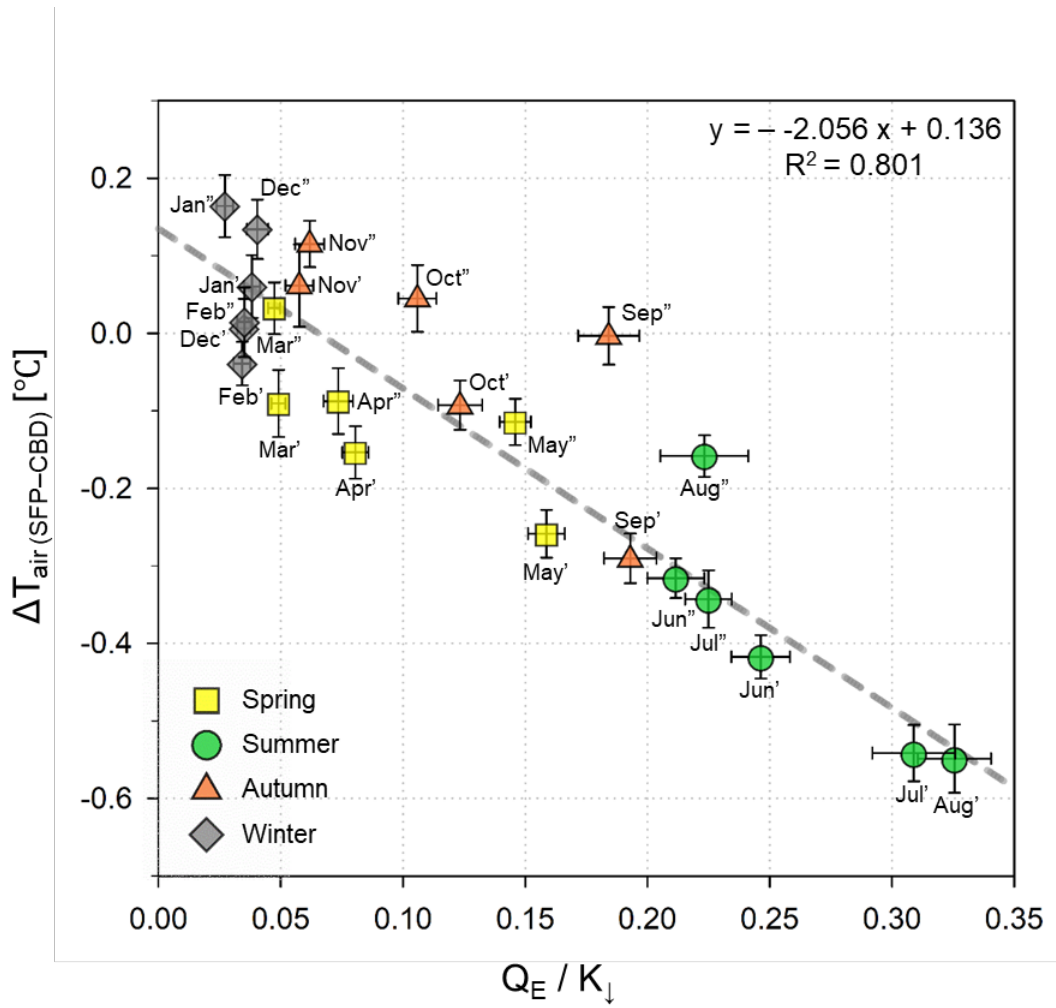
847 Figure 6. Hourly mean diurnal variation of the urban heat island intensity (UHIi) of the SFP and CBD in the  
 848 summer of 2013 and 2014. The error bars represent standard errors.

849



850

851 Figure 7. Mean diurnal pattern of air temperature difference ( $\Delta T_{air}$ ) between CBD and SD in summer (a) before  
 852 and (b) after the construction of the park. CBD indicates an average of three automatic weather stations (Gangnam,  
 853 Seocho, Songpa) in Seoul. The red dash line indicates the mean  $\Delta T_{air}$  before and after the construction of the park.

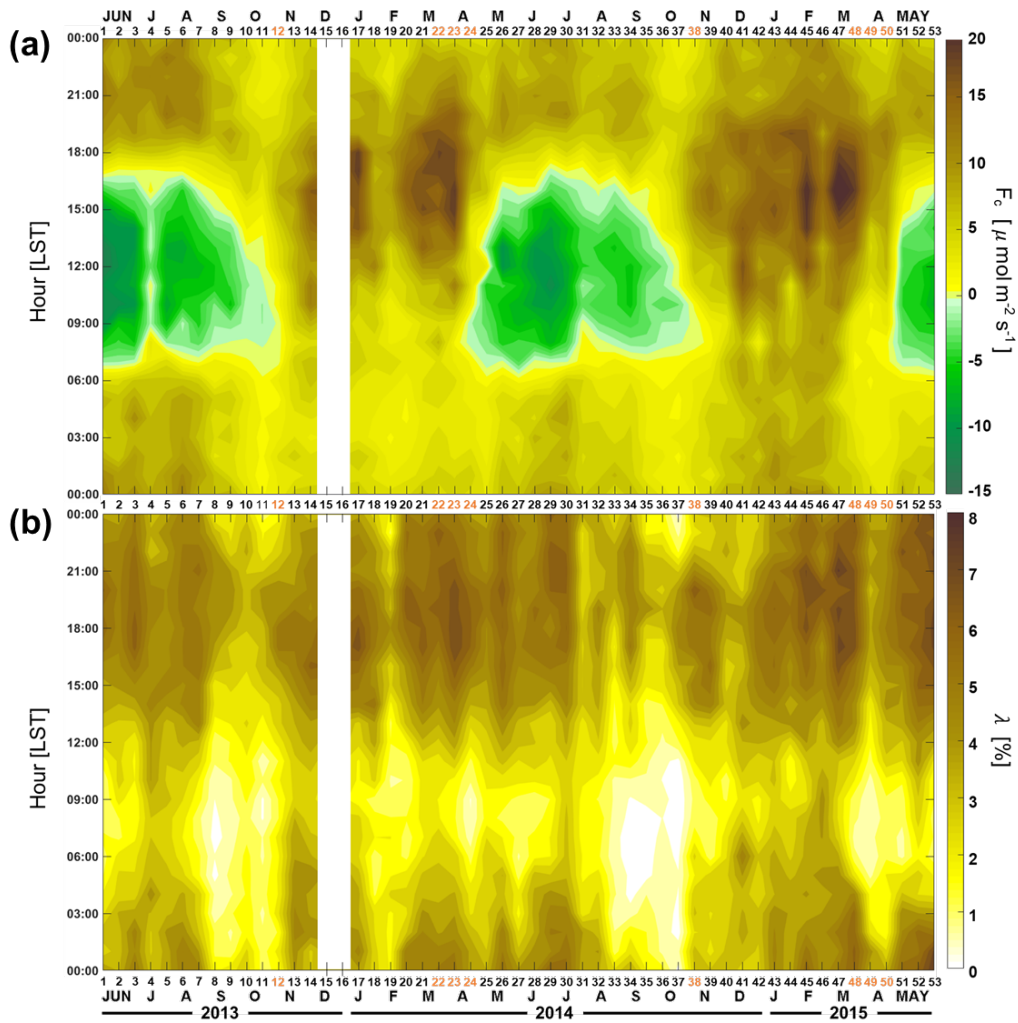


854

855 Figure 8. Relationship between the ratio of monthly  $Q_E$  to  $K_{\downarrow}$  and mean air temperature difference between SFP  
 856 and CBD during the daytime ( $K_{\downarrow} > 120 \text{ W m}^{-2}$ ) for two years. The quotation and double-quotation marks on the  
 857 scatter indicate the first and second year of the observation period, respectively. The error bars represent standard  
 858 errors based on daily values, and the grey dotted line is calculated using linear regression model considering errors  
 859 in both axes (York et al., 2004).

860

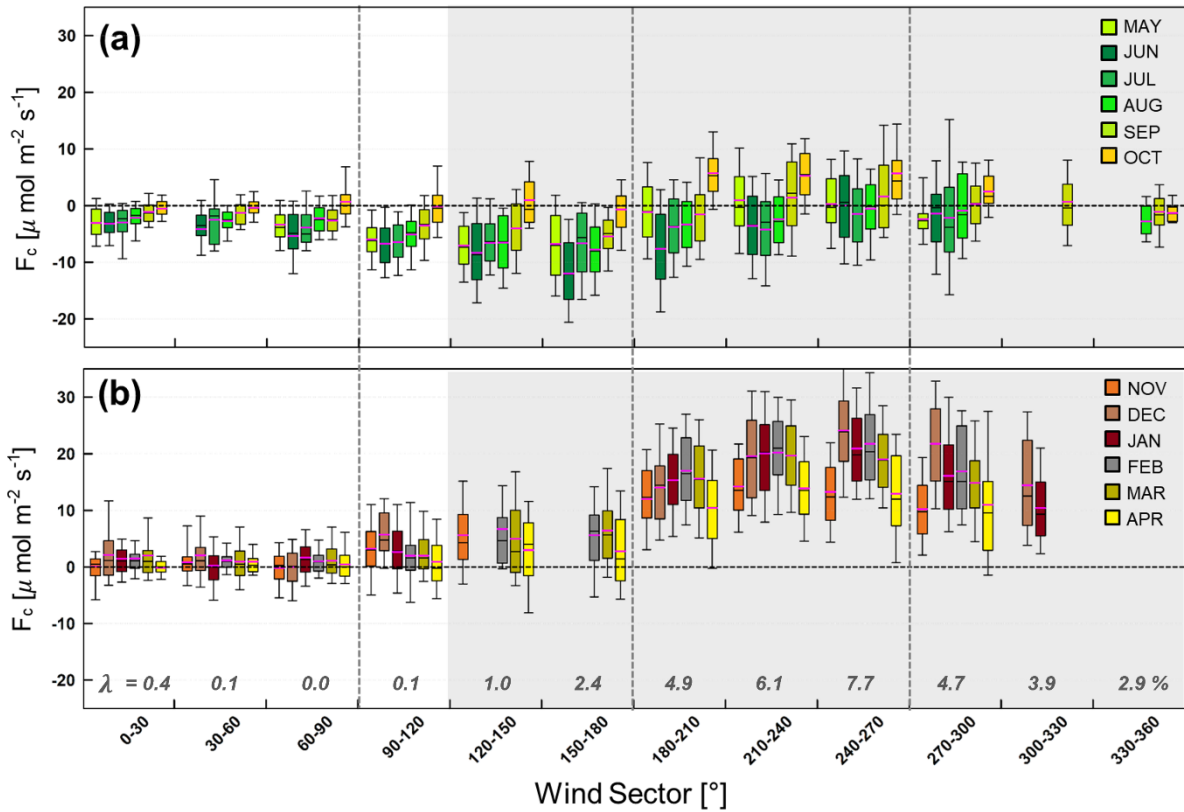
861



862

863 Figure 9. (a) Temporal variation of hourly averaged  $F_C$  and (b) footprint-weighted road fraction ( $\lambda$ ) as every two-  
864 week average (x-axis: the date, y-axis: time of day). In December 2013, there was a gap for approximately 4  
865 weeks due to the power system failure. The yellow numbers in x-axis indicate the transition period when traffic  
866 emissions ( $E_R$ ) contributes to the observed  $F_C$  significantly.

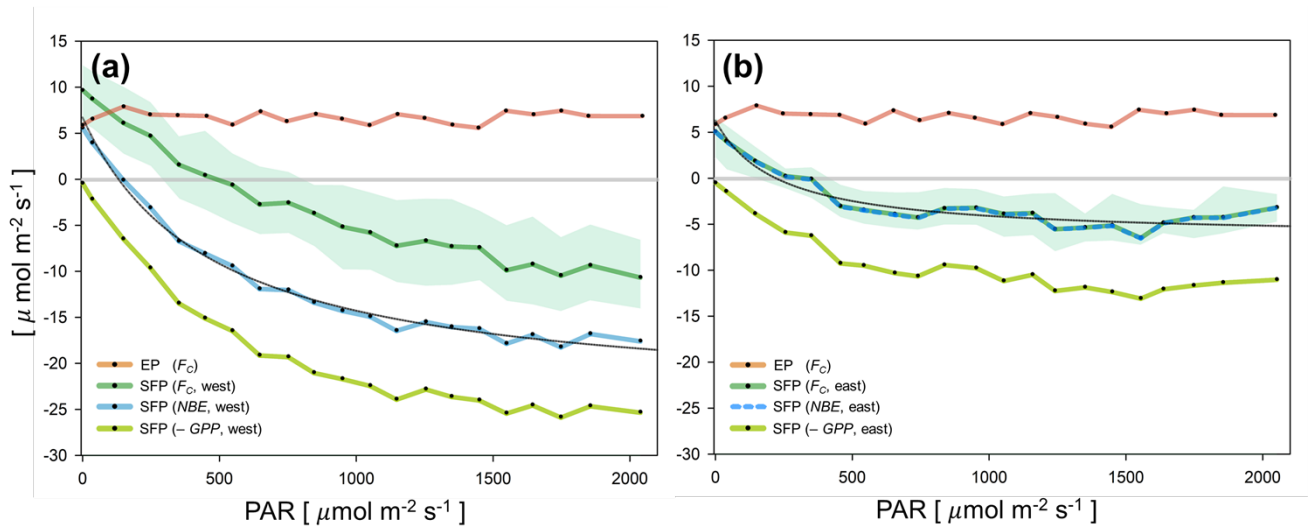
867



868

869 Figure 10. Monthly boxplots of daytime ( $K_t > 120 \text{ W m}^{-2}$ )  $F_c$  by wind direction. Boxes have a minimum of 20  
 870 samples. Box limits are upper and lower quartiles, and whiskers are distances of 1.5 times the interquartile range  
 871 from each quartile. Median and mean values are indicated by the black and pink horizontal lines. The average  
 872 source area weighted road fractions ( $\lambda$ ) are shown below the graph, and wind sectors with  $\lambda$  greater than 1% are  
 873 shaded in gray.





875 Figure 11. During the growing season (June–August 2013, 2014) when  $E_B$  is negligible, light-response curves as a function of photosynthetically active radiation (PAR, in bins of  $100 \mu\text{mol m}^{-2} \text{s}^{-1}$ ): (a) for the western sectors ( $150^\circ < \Phi < 300^\circ$ ) and (b) for the eastern sectors ( $30^\circ < \Phi < 90^\circ$ ). Black line is a rectangular hyperbolic equation fitting net biome exchange ( $NBE = RE - GPP = F_C - E_R$ ) to PAR, and EP (brown line) is a light-response curve for the high-rise high-population residential area in Seoul. The shaded areas indicate interquartile range.

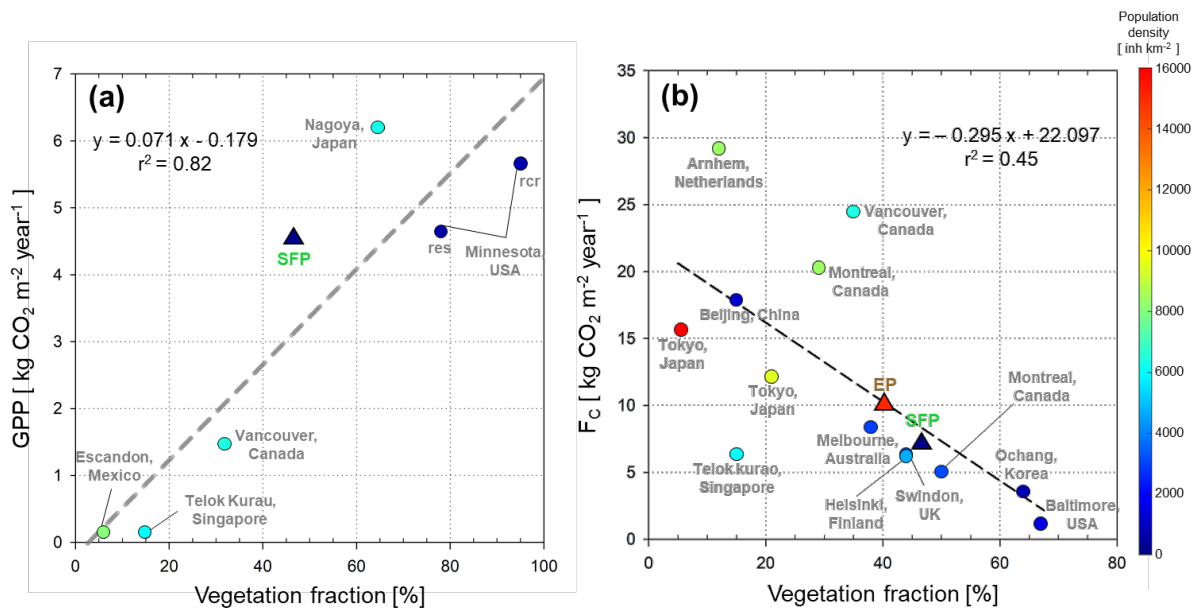
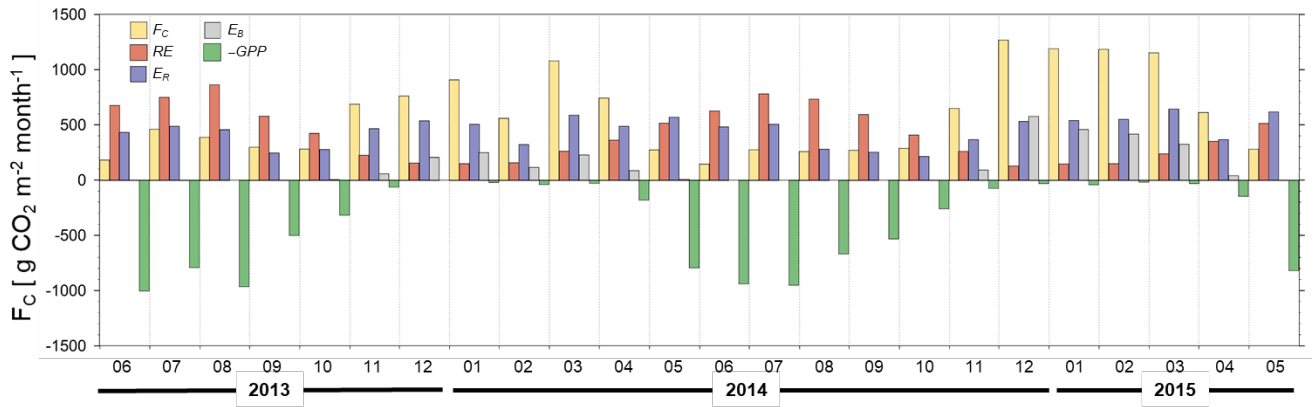


Figure 12. Relationship between vegetation fraction (a) annual *GPP* and (b) annual *F<sub>c</sub>* in urban sites. Dashed line in (a) and (b) indicates a linear regression of *GPP* in urban sites from Awal et al. (2010), Crawford and Christen (2015), Velasco et al. (2016), and Menzer and McFadden (2017) and *NEE* from Hong et al. (2019b) and references therein scaled with vegetation fraction, respectively. See main texts for more information.

885



890 Figure 13. Monthly sums for gap-filled  $F_C$  (yellow bar) with  $RE$  (red bar),  $E_R$  (blue bar),  $E_B$  (gray bar), and  $-GPP$  (green bar).